พฤติกรรมการละลายโดยเคมีไฟฟ้าของแร่ไพไรต์ภายใต้สภาวะที่มีโลหะออกไซด์หรือสารเชิงซ้อนโลหะอินทรีย์: แนวทางสู่การลดผลกระทบน้ำเหมืองเป็นกรด

นายสุชล วีระวัฒนานันท์

วิทยานิพนธ์นี้เป็นส่วนหนึ่งของการศึกษาตามหลักสูตรปริญญาวิศวกรรมศาสตรมหาบัณฑิต
สาขาวิชาวิศวกรรมทรัพยากรธรณี ภาควิชาวิศวกรรมเหมืองแร่และปิโตรเลียม
คณะวิศวกรรมศาสตร์ จุฬาลงกรณ์มหาวิทยาลัย
ปีการศึกษา 2558

Electrochemical behavior of pyrite dissolution in the presence of metal oxides or metal-organic complexes: Pathway to AMD suppression

Mr. Suchol Veerawattananun

A Thesis Submitted in Partial Fulfillment of the Requirements
for the Degree of Master of Engineering Program in Georesources Engineering
Department of Mining and Petroleum Engineering
Faculty of Engineering
Chulalongkorn University
Academic Year 2015

Thesis Title	Electrochemical behavior of pyrite dissolution in the presence of metal oxides or metal-organic complexes: Pathway to AMD suppression
By	Mr. Suchol Veerawattananun
Field of Study	Georesources Engineering
Thesis Advisor	Associate Professor Dawan Wiwattanadate, Ph.D.

Accepted by the Faculty of Engineering, Chulalongkorn University in Partial Fulfillment of the Requirements for the Master's Degree

.....Dean of the Faculty of Engineering
(Associate Professor Supot Teachavorasinskun, Ph.D.)

THESIS COMMITTEE

.....Chairman
(Assistant Professor Thitisak Boonpramote, Ph.D.)
.....Thesis Advisor
(Associate Professor Dawan Wiwattanadate, Ph.D.)
.....External Examiner
(Associate Professor Pinyo Meechumna, Ph.D.)

สุชล วีระวัฒนานันท์ : พฤติกรรมการละลายโดยเคมีไฟฟ้าของแร่ไพไรต์ภายใต้สภาวะที่มีโลหะออกไซด์หรือสารเชิงซ้อนโลหะอินทรีย์: แนวทางสู่การลดผลกระทบน้ำเหมืองเป็นกรด (Electrochemical behavior of pyrite dissolution in the presence of metal oxides or metal-organic complexes: Pathway to AMD suppression) อ.ที่ปรึกษาวิทยานิพนธ์หลัก: รศ. ดร. ดาวัลย์ วิวรรธนะเดช, 51 หน้า.

ไพไรต์ ซึ่งเป็นแร่ซัลไฟด์ชนิดหนึ่งที่พบมากที่สุดในธรรมชาติ เป็นต้นเหตุหลักของการเกิดน้ำเหมืองเป็นกรด (AMD) ซึ่งปล่อยน้ำชะที่มีความเป็นกรดสูงและปนเปื้อนด้วยโลหะหนักสู่ทางน้ำธรรมชาติ จึงเป็นหนึ่งในผลกระทบสิ่งแวดล้อมอันร้ายแรงจากกิจกรรมเหมืองแร่ที่ต้องจัดการอย่างเหมาะสม โดยทั่วไปการละลายของแร่ไพไรต์เป็นกระบวนการทางเคมีไฟฟ้า ซึ่งประกอบด้วยการละลายของแร่ไพไรต์ที่ขั้วแอโนดและการถูกรีดิวซ์ของตัวออกซิไดส์ที่ขั้วแคโทดบนพื้นผิวของแร่ไพไรต์ วิทยานิพนธ์ฉบับนี้ได้ทำการศึกษาและรายงานผลการศึกษาพฤติกรรมการละลายของแร่ไพไรต์ อิทธิพลของโลหะออกไซด์ (เฮมาไทต์ และอะลูมินา) และสารประกอบเชิงซ้อนโลหะอินทรีย์บางชนิด (ทิเทเนียมและซิลิกอนแคติคอล) ที่มีต่อการละลายของไพไรต์

แร่เฮมาไทต์ถูกเลือกเป็นตัวแทนโลหะออกไซด์ในการศึกษาครั้งนี้เนื่องจากเป็นหนึ่งในผลิตภัณฑ์สุดท้ายของกระบวนการละลายของแร่ไพไรต์ ส่วนอะลูมินาถูกเลือกมาในฐานะตัวแทนของแร่กลุ่มอะลูมิโนซิลิเกตที่พบได้โดยทั่วไปในธรรมชาติ ผลของการศึกษาอิทธิพลของเฮมาไทต์และอะลูมินาต่อการการละลายของแร่ไพไรต์พบว่าการละลายของแร่ไพไรต์ลดลงในสภาวะที่มีเฮมาไทต์ แต่ลดลงในสภาวะการละลายที่มีอะลูมินา ส่วนผลการศึกษาทางเคมีไฟฟ้าโดยใช้ขั้วไฟฟ้าที่ทำจากผลึกของแร่ไพไรต์บ่งชี้ว่าปฏิกิริยาครึ่งเซลล์ด้านแอโนดเพิ่มขึ้นทั้งในสภาวะที่มีเฮมาไทต์หรืออะลูมินา ขณะที่ปฏิกิริยาครึ่งเซลล์ด้านแคโทดลดลงเนื่องจากการเกาะติดของอนุภาคโลหะออกไซด์บนแร่ไพไรต์ไปลดหรือบดบังพื้นที่สัมผัสทางกายภาพระหว่างแร่ไพไรต์กับตัวออกซิไดส์

การกักเก็บขนาดเล็กโดยใช้พาหะ เป็นเทคนิคในการปกป้องแร่ไพไรต์โดยประยุกต์ใช้สารเชิงซ้อนโลหะอินทรีย์ในการยับยั้งการออกซิไดส์ของแร่ไพไรต์และเปลี่ยนคุณสมบัติพื้นผิวของแร่ไพไรต์ ในการศึกษานี้เสียรภาพของสารเชิงซ้อนโลหะแคททีคอลทั้งในสารละลายและบนแร่ไพไรต์ได้รับการตรวจสอบเพื่อเป็นการศึกษาขั้นพื้นฐานสำหรับงานวิจัยต่อไปในอนาคต ผลการศึกษาพบการมีอยู่ของสารเชิงซ้อนโลหะแคททีคอลในสภาวะความเป็นด่าง

ภาควิชา วิศวกรรมเหมืองแร่และปิโตรเลียม ลายมือชื่อนิสิต .....

สาขาวิชา วิศวกรรมทรัพยากรธรณี ลายมือชื่อ อ.ที่ปรึกษาหลัก .....

ปีการศึกษา 2558

5770328421 : MAJOR GEORESOURCES ENGINEERING
KEYWORDS: ACID MINE DRAINAGE (AMD) / PYRITE / PYRITE DISSOLUTION / HEMATITE / ALUMINA / METAL-ORGANIC COMPLEXES / CYCLIC VOLTTAMMETRY / CHRONOAMPEROMETRY / METAL OXIDE

SUCHOL VEERAWATTANANUN: Electrochemical behavior of pyrite dissolution in the presence of metal oxides or metal-organic complexes: Pathway to AMD suppression. ADVISOR: ASSOC. PROF. DAWAN WIWATTANADATE, Ph.D., 51 pp.

Pyrite, one of the most abundant metal sulfide minerals found in nature, is considered as main cause of a serious anthropogenic environmental impact caused by mining activities known as acid mine drainage (AMD), releasing highly acidic leachate contaminated with various heavy metals and contaminating natural waterway. In general, dissolution process of pyrite is an electrochemical phenomenon, of which pyrite dissolution at anode and reducing oxidants at cathode on the pyrite surface. Study results on effects of common metal oxides, like hematite (α-Fe_2O_3) and alumina (α-Al_2O_3), which naturally come to contact with pyrite at the AMD contaminated sites, and also preliminary study results on redox behavior and stability of metal-organic complexes (i.e. Ti- and Si-catechol complexes) on the pyrite surface are reported in this thesis.

The hematite was chosen for this study because it is one of the main final products from pyrite dissolution process and the alumina was chosen as a representative of alumino-silicate minerals commonly found in nature. Results of the study on effects of hematite and alumina on pyrite dissolution dynamics based on batch-type experiment indicated the pyrite dissolution decreased with the presence of hematite but increased with the presence of alumina. Upon electrochemical study using pyrite crystal electrode, it was found that anodic half-cell reaction of pyrite dissolution was enhanced with the presence of either hematite or alumina. Whereas, the cathodic half-cell reaction was lessened due to the attached metal oxide particles physically reduce contact area between the pyrite and oxidants.

Carrier Microencapsulation is a pyrite passivation technique that utilize metal-organic complexes to suppress pyrite oxidation and change pyrite's surface condition. In this study, stability of metal-catechol complexes in solution and on pyrite were evaluated as fundamental study for further researches in the future. The results confirmed the presence of metal-catechol complexes in alkaline solution.

Department:	Mining and Petroleum Engineering	Student's Signature	.....
		Advisor's Signature	.....
Field of Study:	Georesources Engineering		
Academic Year:	2015		

ACKNOWLEDGEMENTS

This thesis owns insurmountable debts for its existence to the help, support and inspiration of several sections. Firstly, I also feel thankful and would like to acknowledge the graduate program for fostering frontiers of practical solutions in a Population-Activities-Resources-Environments (PARE) chain at Hokkaido University (Japan) for their efforts and financial supports to bring students from different countries to meet and develop with each other. As the time I spent with "PARE" friends was so valuable, we were able to support each other over hard works and enjoy memorable events. I also would like to thank the Thai student community in Hokkaido for creating warmhearted atmosphere for everyone.

I also would like to convey my gratitude oversea to Laboratory of Mineral Processing and Resources Recycling, Division of Sustainable Resources Engineering, Graduate School of Engineering, Hokkaido University including their staffs and students those took care, taught and experienced many things with me during my exchange. For this occasion, I wholeheartedly thank Asst. Prof. Dr. Carlito Baltazar Tabelin and his students for their patience and guidance in this research and also for thoroughly corrected and revised my conference manuscripts including this thesis. I also would like to express my grateful thoughts to Prof. Dr. Naoki Hiroyoshi and Assoc. Prof. Dr. Mayumi Ito for taking care of me and always arranging seminars with interactive learning and researching environment. Most importantly, all of the mentioned wonderful environment could not be perfected without all students in the laboratory those always be friendly and cheerful at all time.

The thesis definitely could not serve its purpose without hospitalities from my thesis committee members. I would like to gratefully express all my sincere thanks to my thesis advisor, Assoc. Prof. Dr. Dawan Wiwattanadate, for all her kindness, suggestions and guidance during the fabrication of this thesis. I also would like to convey my greatest gratitude to Assoc. Prof. Dr. Pinyo Meechumna and Asst. Prof. Dr. Thitisak Boonpramote for all their educative, supportive and enlightenful advises over the past few years since I was a bachelor student.

I also really appreciated supports from other staffs at Department of Mining and Petroleum Engineering, Faculty of Engineering, Chulalongkorn University for my documentations. I could not graduate and finish this thesis without hospitalities and advises from every friends and seniors at the department those overcame numerous obstacles together when we had hard times.

Last but not least, my deepest gratitude definitely goes to the most important component in my life – my family. For them, I would like to express my sincerest gratitude for unconditional love and supports throughout my whole life. Because of them, I can become me as I am today.

CONTENTS

Page

LIST OF FIGURES

LIST OF TABLES

CHAPTER 1

INTRODUCTION

Acid mine drainage (AMD) is one of the most concerned environmental impact mainly caused by anthropogenic activities, generally from mining and mineral processing activities, in both active and abandoned mines (Evangelou, 1995; Johnson & Hallberg, 2005; Lowson, 1982; Rimstidt & Vaughan, 2003). In some occasions, AMD is referred as acid rock drainage (ARD), since underground mines, waste rock dumps, overburden piles, tailings dams and tunnel excavations for construction of road and railways (Egiebor & Oni, 2007; Tabelin, Igarashi, Tamoto, & Takahashi, 2012)are also sources of acid drainage generations.

AMD/ARD is generated as sulfide minerals are exposed to atmospheric conditions (oxygen and water). Pyrite (FeS_2), as the most abundant metal sulfide mineral in earth's crust, can be found in various geological formations and also usually found as associated mineral within base metal sulfide ore formations (i.e. chalcopyrite ($CuFeS_2$), sphalerite ((Zn,Fe)S) and galena (PbS)) (Chandra & Gerson, 2010).In mining perspective, pyrite is normally rejected as gangue mineral due to its low utility and economical value and classified as waste rocks, overburden or either goes to the tailings dam after processing process. Pyrite also contains other elements within its mineral lattice and some of the elements (*i.e.* As) can be threatening to the metal smelting plants and resulted as "penalty" charges that reduce the ore value (Abraitis, Pattrick, & Vaughan, 2004).

Gray (1997) listed example of sulphide minerals associated with AMD formation in Avoca region as illustrated in table 1-1.

Acid mine drainage (AMD) is considered as a devastating environmental problem because once AMD was generated, it releases highly acidic leachate with high concentrations of sulfate, iron, base metals and other hazardous elements those are presence in the mineral lattice (*i.e.* Cd, Hg, Pb and As). Once the acidic drainage is leached out, it flows through natural waterways, contaminates soil, run-off water and groundwater and affects wellbeing and ecosystems around the contaminated sites (Akcil & Koldas, 2006).

Table 1-1Major minerals associated with AMD in Avoca region, Australia (Gray, 1997)

Mineral	Composition	Mineral	Composition
Arsenopyrite	FeAsS	Millerite	NiS
Bornite	$CuFeS_4$	Mobybdenite	MoS_2
Chalcocite	Cu_2S	Pyrite	FeS_2
Chalcopyrite	$CuFeS_2$	Pyrrhhdite	$Fe_{11}S_{12}$
Covellite	CuS	Sphalerite	ZnS
Galena	PbS		

Järup (2003) reviewed health effects of heavy metal exposure to Cadmium (Cd), Mercury (Hg), Lead (Pb) and Arsenic (As) as summarized in table 1-2:

Table 1-2 Health risks upon heavy metals (Cd, Hg, Pb and As) exposure (Järup, 2003)

Type of contaminant	Health effects on human
Cadmium (Cd)	Kidney damage / cancer Itai-itai disease (Long term exposure)
Mercury (Hg)	Lung/kidney damage (Inorganic mercury) Paresthesia / Numbness (Organic mercury)
Lead (Pb)	Headache, irritability, abdominal pain and other symptoms related to nervous system Kidney damage (Long term exposure)
Arsenic (As)	Gastrointestinal symptoms Disturbance of cardiovascular / central nervous system Lung / kidney / bladder cancer

It is well-known problem that AMD is a large scale environmental problem in many developed countries with numerous abandoned mines and currently require remediation from government as acid drainage normally comes into light years after mine closure period. For example, in the western U.S., there was a report that more than 20,000 abandoned mines affecting 8,000 – 16,000 kilometers of steamways (U.S. Environmental Protection Agency, 1994).

1.1 Thesis objectives

The thesis objectives are as follows:

(i) To investigate the effects and electrochemical reactions of metal oxide (hematite and alumina) micro-particles on pyrite dissolution

(ii) To investigate the effects and electrochemical reactions of metal oxide complexes (Ti- and Si-catechol complexes) and pyrite in an AMD passivation technique called Carrier Microencapsulation (CME)

1.2 Outline of this thesis

This thesis is composed of four chapters with appendix

Chapter 1 contains brief introduction of acid mine drainage (AMD) and its environmental concerns, which will be the context of this thesis.

Chapter 2 reviews previous studies of pyrite dissolution mechanism and AMD remediation options.

Chapter 3 presents the characterization of experimental materials and methodology for the study of effects of hematite (α-Fe_2O_3) and alumina (α-Al_2O_3) on pyrite dissolution. Some preliminary results for determining the working conditions are also presented in this chapter.

Chapter 4 shows results and discussion of the study of effects of hematite (α-Fe_2O_3) and alumina (α-Al_2O_3) on pyrite dissolution.

Section 4.1 introduces the result on the oxidation products of pyrite in air and deionized water as a control case.

Section 4.2 shows the results and discussion on the effects of hematite on pyrite dissolution in details.

Section 4.3 focused on the results of the effects of alumina on pyrite dissolution process.

Chapter 5 concludes the findings of this thesis.

In **Appendix**, electrochemical studies of pyrite oxidation in the presence of metal-organic complexes were conducted. Redox properties of free-catechol and metal-catechol complexes in solution and on pyrite were examined using cyclic voltammetry.

CHAPTER 2
LITERATURE REVIEW

2.1 Review on pyrite and its dissolution mechanism

Pyrite (FeS_2), iron disulfide, has a crystal form of face-centered cubic (FCC). Similar to that of the halite (NaCl), in the structure of pyrite, ferrous (Fe^{2+}) cation is located in the same position as Na^+ in halite crystal and S_2^{2-} anion is located at the position of Cl^- in halite crystal (Murphy & Strongin, 2009) as illustrated in figure 2-1. It is also reported that presence of trace elements in pyrite lattice can affects properties and reactivity of pyrite (Chandra & Gerson, 2010).

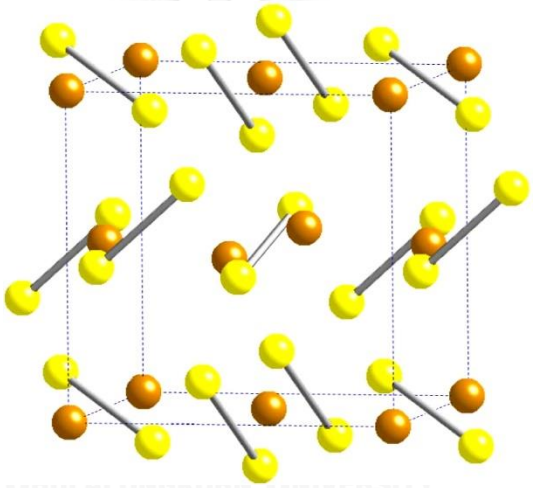

Figure 2-1 Atomic schematic model of pyrite unit cell. Brown spheres represent Fe and yellow spheres represent S (Murphy & Strongin, 2009)

By the 1960s, the dissolution process of pyrite was well-accepted as a direct adsorption chemical dissolution process. Lowson (1982) reviewed and summarized the studies of pyrite dissolution in aqueous prior to 1982 into great details. The oxygen adsorption chemical dissolution pathway of pyrite dissolution comprises of 3 reactions as follows:

(1) The oxidation of pyrite by adsorbed molecular oxygen to produce ferrous (Fe^{2+}) and sulfate (SO_4^{2-})
(2) The oxidation of ferrous (Fe^{2+}) to ferric (Fe^{3+}), which is reported to be "rate determining step" of pyrite dissolution process (Singer & Stumm, 1970)
(3) The oxidation of pyrite by ferric (Fe^{3+}) produced from the previous step

Afterward, stable oxygen isotope study of pyrite oxidation by isotopically pure $^{18}O_2$ and $H_2{}^{16}O$ was done to trace the source of oxygen in the oxidation products (SO_4^{2-}) whether it came from oxygen or water. It was found that molecular oxygen in the sulfate product was derived from that of water molecule, not dissolved oxygen (Reedy, Beattie, & Lowson, 1991). The finding was quite contradicting with the previous mechanism of oxygen adsorption, in which the oxygen molecules of the end product should dominantly derived from dissolved oxygen.

Rimstidt and Vaughan (2003) reviewed the electrochemical pathway of pyrite oxidation as the mechanism composes of 3 steps as follows:

(1) Reduction of oxidants (O_2 and Fe^{3+}) at cathodic sites on pyrite surface described by following reactions:

$0.5\ O_2 + 2H^+ + 2e^- \rightarrow H_2O$ equation 2-1

$Fe^{3+} + e^- \rightarrow Fe^{2+}$ equation 2-2

This step is considered to be "rate determining step" of the whole dissolution mechanism (Williamson & Rimstidt, 1994).

(2) Transfer of electrons through semiconductor property of pyrite from anodic sites to cathodic sites, where the electrons are transferred to oxidants as explained above.

(3) Oxidation of pyrite at anodic sites, where electrons are removed from sulfur species as generally shown in following reaction:

$FeS_2\ (s) + 8\ H_2O \rightarrow 16\ H^+ + 2SO_4^{2-} + 14e^-$ equation 2-3

As 7 electrons are needed to be removed from disulfide (S_2^{2-}) and 8 electrons are needed in the case of sulfide (S^{2-}) to form sulfate (SO_4^{2-}). The oxidation of sulfur species (equation 2-3) actually comprises many elementary reactions, which transfer 1 electron at a time and also produce of intermediate species (*i.e.* $S_2O_3^{2-}$) on the process.

Note that the component that is oxidized is the sulfur species only, the iron (Fe^{2+}) in the pyrite is not oxidized and dissolved as Fe^{2+} into the solution.

So, by combining equation 2-1, 2-2 and 2-3, the overall reaction of electrochemical dissolution of pyrite can be described as:

$FeS_2\ (s) + 3.5\ O_2 + H_2O \rightarrow Fe^{2+} + 2\ H^+ + 2\ SO_4^{2-}$ equation 2-4

$FeS_2\ (s) + 14\ Fe^{3+} + 8\ H_2O \rightarrow 15\ Fe^{2+} + 16\ H^+ + 2\ SO_4^{2-}$ equation 2-5

In the next section, microencapsulation technique, a technique that suppress the contact between pyrite and oxidants, will be briefly reviewed.

2.2 Brief review on pyrite microencapsulation technologies

Microencapsulation technique is a pyrite passivation technique which aimed to suppress pyrite dissolution by covering pyrite surface with impermeable protective coatings to reduce oxygen diffusion and minimize the overall pyrite oxidation rate (Evangelou, 1995).The first application of microencapsulation is to form phosphate or silica coating on pyrite surface by using H_2O_2 or hypochlorite as an oxidizing reagent to accelerate the production of Fe^{3+}, then the Fe^{3+} may form impermeable phosphate or silica coating with KH_2PO_4 or H_4SiO_4 respectively (Evangelou, 2001).

Recently, carrier microencapsulation (CME), a microencapsulation technique that utilizes organic carrier to form a coating on pyrite surface had been reported and that Ti^{4+} ion extraction from Ti-bearing minerals using catechol (1,2-dihydroxybenzene, $C_6H_4(OH)_2$) was possible and a stable Ti-catechol complex ($Ti(cat)_3^{2-}$) could be formed. On the pyrite surface, this complex is oxidized and $Ti(OH)_4$ or TiO_2 coating was formed that suppressed pyrite oxidation (Satur, Hiroyoshi, Tsunekawa, Ito, & Okamoto, 2007). The mechanism of CME is illustrated in figure 2-2. Another researcher modified this technique to form SiO_2 coating on the pyrite surface with Si-catechol complex ($Si(cat)_3^{2-}$) that not only minimized pyrite oxidation but also suppressed the floatability of pyrite during coal flotation (Jha, Satur, Hiroyoshi, Ito, & Tsunekawa, 2008, 2011; Thakur Jha, Satur, Hiroyoshi, Ito, & Tsunekawa, 2012).

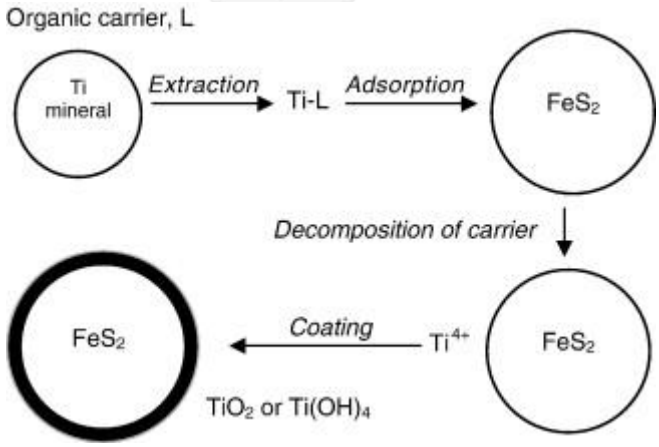

Figure 2-2 Mechanism of carrier microencapsulation using Ti-catechol complex (Satur et al., 2007)

CHAPTER 3
MATERIALS AND METHODS

In chapter 3 and 4, the effects of metal oxides those frequently come into contact with pyrite are elucidated with series of batch-type leaching experiment, electrochemical studies, surface-sensitive characterization and geochemical modelling calculations. The metal oxides chosen for this study are hematite (α-Fe_2O_3) and alumina (α-Al_2O_3).

As pyrite dissolves, the oxidation products will be subjected to changes and form into more thermodynamically stable product. For the final product of pyrite dissolution at low temperature (< 1173-1273 K) and high oxygen concentration circumstance, the final product of pyrite decomposition was reported to be hematite (Hu, Dam-Johansen, Wedel, & Hansen, 2006).

Aluminum is considered as the second-most abundant element in the Earth's crust (with Al_2O_3 weight percentage of 16% in the continental crust) (Taylor, 1964).

For this instance, hematite and alumina would strongly influence the overall dynamics of pyrite oxidation in the environment.

3.1 Characterization of pyrite, hematite and alumina samples

3.1.1 Chemical and mineralogical characterization of pyrite

Pyrite sample from Cerro de Pasco mine, Peru was used in this study. First, visible impurities on pyrite were removed manually after rough crushing of the sample with a hammer. Some of the large well-defined pyrite crystals were kept for the electrochemical experiments as material for the single-crystal pyrite electrode, the preparation of which will be explained later. The rest of the sample was crushed and classified to +500-750 µm for characterization and batch experiments.

For characterization of the sample, washed pyrite sample (details of the washing technique will be describe later on) was further crushed using agate mortar to less than 50 µm to identify its mineral composition by X-ray powder diffraction (MultiFlex, Rigaku Corporation, Japan). For the chemical composition analysis, three pyrite samples (< 50 µm) of ca. 0.1 g were dissolved in 5 ml of 12M HCl and 3 ml of 16M HNO_3 (Wako Chemical Co. Ltd.) using microwave acid digestion (Ethos, Milestone Inc., USA) and the concentrations of different elements dissolved in the leachates were measured by inductively coupled plasma atomic emission spectrometer (ICP-AES) (ICPE-9800, Shimadzu Corporation, Japan). The standard solutions used for the calibration curve of the measurement were prepared and diluted from 1000 ppm standard metal solutions (Wako Chemical Co. Ltd.). As some elements are not

supposed to be mixed together in one standard, 4 sets of standard solutions were prepared to measure 10 different dissolved elements in the leachate: (1) Fe standard solution, (2) Si standard solution, (3) Ca/K/Na/Mg mixture standard solution, and (4) Cu/Zn/As/Al mixture standard solution. The portion of S in each pyrite sample was then derived as the remaining amount other than the measured elements.

According to the XRD pattern shown in figure 3-1, the pyrite sample used in this study was relatively pure as indicated by the strong peaks of the mineral without any significant peaks of other common associated minerals (*e.g.* quartz). This statement is also supported by the chemical analysis (averaged value between the 3 samples) as illustrated in figure 3-2, which shows that the molar ratio of S to Fe is ca. 2 corresponding to the chemical formula of pyrite (FeS_2).

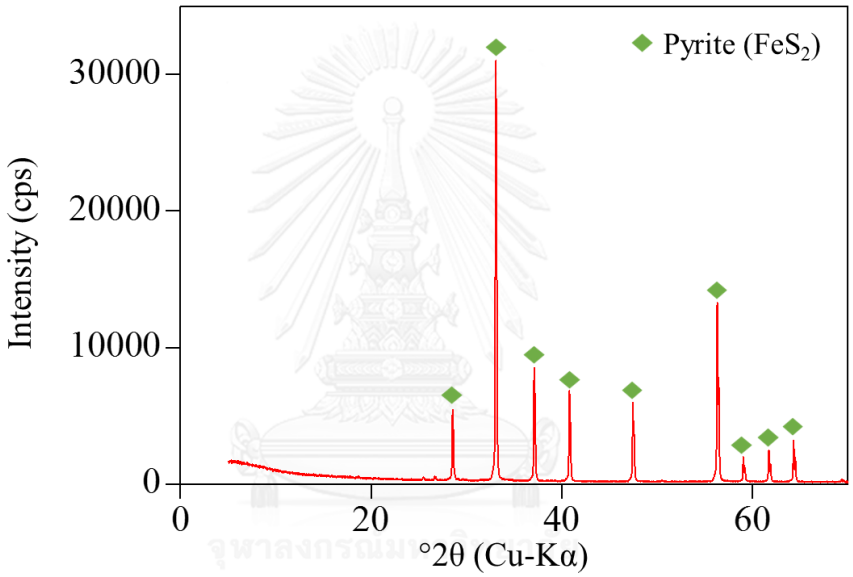

Figure 3-1 XRD Pattern of pyrite sample

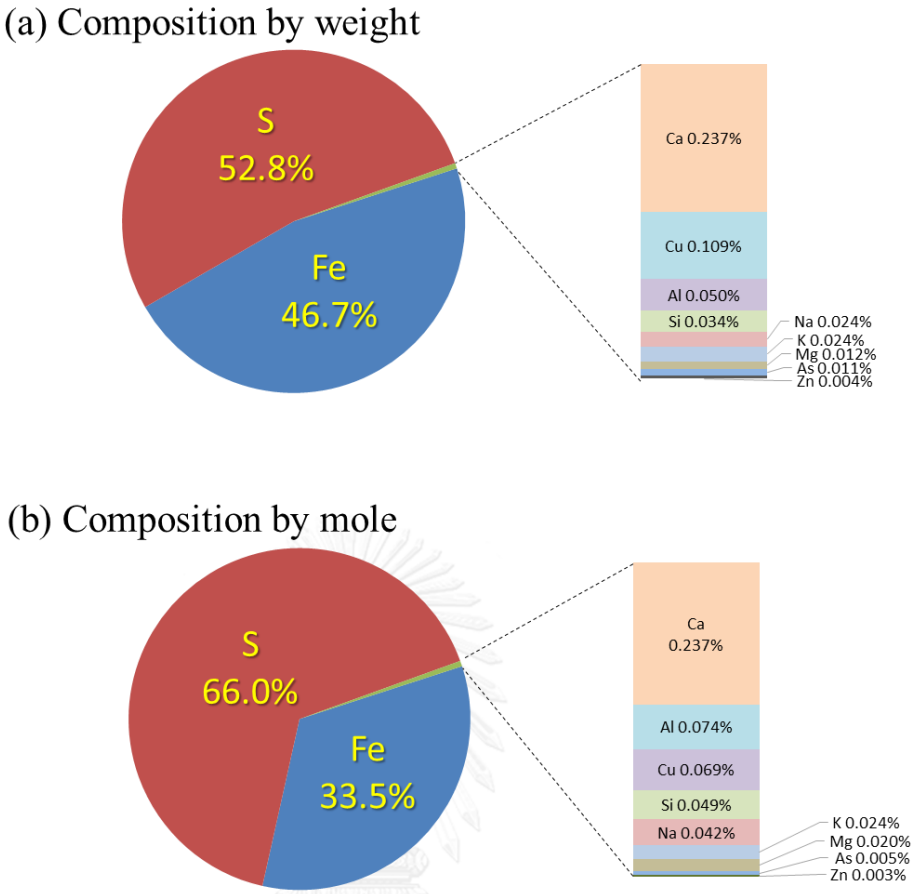

Figure 3-2 Chemical composition of pyrite sample by weight percentage (a) and by molar percentage (b)

3.1.2 Particle size distribution of hematite and alumina sample

Hematite powder (α-Fe_2O_3) used in this study was 99.9% reagent-grade obtained from Wako Pure Chemical Industries, Ltd. (Japan). Micron-sized alumina particles were prepared by grinding 99.9% reagent-grade alumina (α-Al_2O_3) (Wako Chemical Co. Ltd., Japan) with a disc mill (RS100, Retsch Inc., Germany) for 1 minute.

The particle size distributions of the metal oxides were measured using LASER diffraction (Microtrac® MT3300SX, Nikkiso Co., Ltd., Japan). In this study, 200 mg/l of metal oxide suspension was prepared by mixing the corresponding metal oxide powder (hematite or alumina) with deionized water.

Figure 3-3 illustrated that the particle size distribution of hematite and ground alumina was from 0.6-50 µm and 0.3-20 µm with D_{50} at ca. 9.1 µm and 4.1 µm respectively.

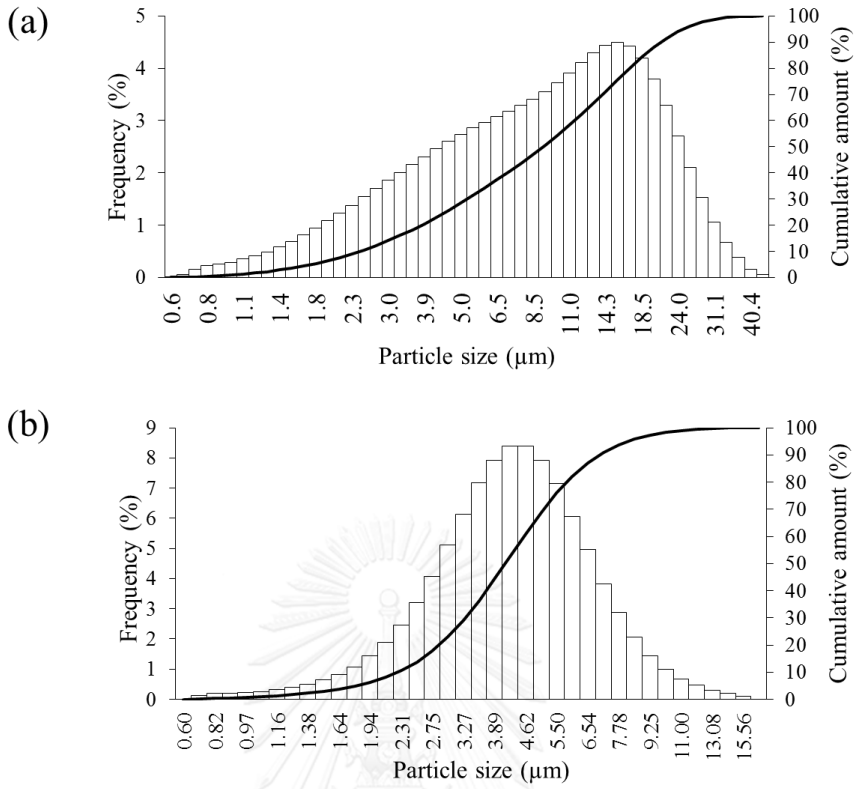

Figure 3-3 Particle size distribution of hematite (a) and alumina (b)

3.1.3 Zeta potential distribution and surface charge

Because physical interaction between metal oxide particles (*e.g.* hematite and alumina) and pyrite in solution are strongly influenced by net surface charges on their surfaces, their zeta potential distributions from pH 3 to 12 were determined using Zetasizer Nano-series with MPT-2 multi-purpose titrator system (Malvern Corporation, UK). Zeta potential distribution measurements over different pH values were performed by adding either 0.1 M HCl or 0.1 M NaOH to adjust the pH.

Pyrite is easily oxidized during the measurement that could affect the net surface charge, so its zeta potential distribution was measured under both oxic (with O_2) and anoxic (without O_2) conditions. Measurement of anoxic condition was done in order to determine the zeta potential of fresh pyrite surface. In the anoxic measurement, freshly ground and washed pyrite sample was mixed into pH-adjusted deionized water, which was purged with N_2 gas for 20 minutes beforehand, then the fresh pyrite suspension was re-purged with N_2 gas for another 10 minutes, ultrasonically dispersed and then immediately analyzed one at a time.

Figure 3-4 illustrates zeta potential distribution of pyrite under oxic and anoxic condition. The measurement under anoxic condition indicates negative net surface charge on fresh pyrite surface between pH 3and 12. On the other hand, as pyrite is oxidized, its net surface charge drastically changed from negative to positive between pH 4 and 8. This change could be attributed to the formation of positively charged iron oxyhydroxides (*e.g.* $Fe(OH)_2^+$, $Fe(OH)^{2+}$) on the pyrite surface during oxidation, which occur easily especially on fresh pyrite surface (Fornasiero, Eijt, & Ralston, 1992).

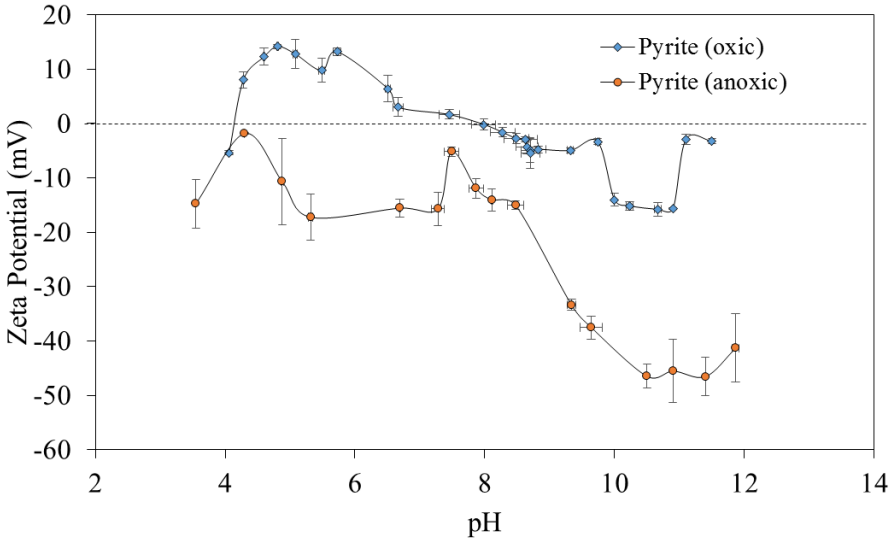

Figure 3-4 Zeta potential distribution of pyrite

The zeta potential distribution of washed pyrite and hematite in deionized water is shown in figure 3-5. The result indicates that the net surface charge of hematite is positive at pH below 8.7, which is opposite to that of fresh pyrite surface. This difference verifies the possibility of attachment of hematite particles onto pyrite surface as confirmed later by 3D microscopic images of pyrite surface after 7 days in DI water or 200 mg/l hematite suspension (Figure 4-9).

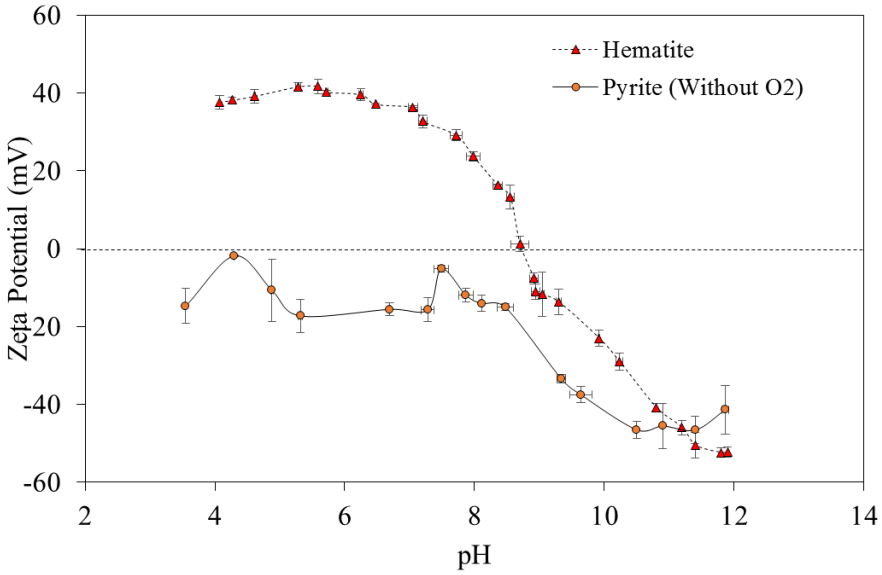

Figure 3-5 Zeta potential of pyrite and hematite in deionized water

The zeta potential distribution of washed pyrite and alumina in deionized water is shown in figure 3-6. The result indicates that net surface charge on hematite is positive at pH below 9.

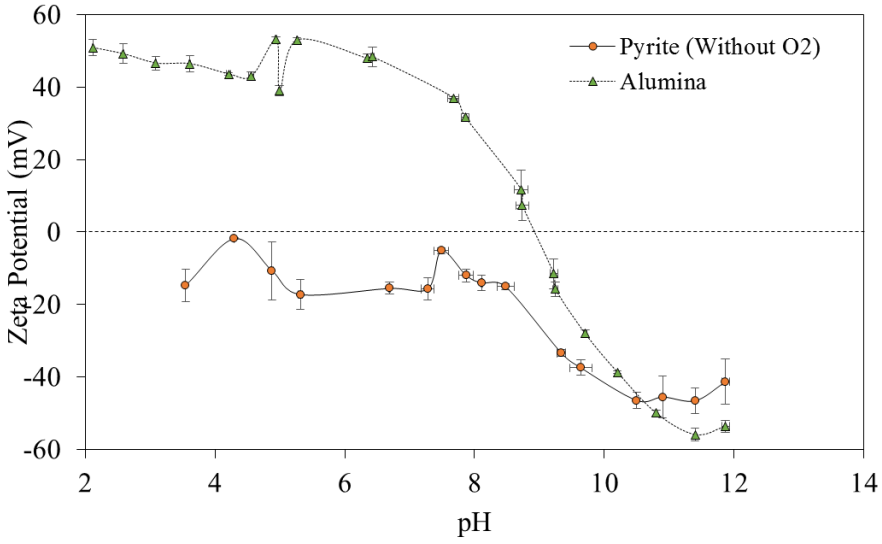

Figure 3-6 Zeta potential of pyrite and alumina in deionized water

3.2 Batch leaching experiments

As fresh pyrite surface is quite reactive and likely to be coated with thin oxidized layer of the oxidation products during the preparation and storage, the pyrite sample was

washed following method to remove the oxidized layer (McKibben & Barnes, 1986). The washing procedure involves a series of steps in which the sample was ultrasonically cleaned in ethanol, washed with 1 M HNO3, rinsed with deionized water, dewatering with acetone and dried in vacuum. The deionized water (DI water) used in every experiments has a resistance of 18.2 $M\Omega \cdot cm^2$.

For the batch-type experiments, 1 g of washed pyrite was mixed with 10 ml of deionized water or 200 mg/l metal oxide suspension (hematite or alumina) in 50 ml Erlenmeyer flasks. These were then shaken under oxic condition at a constant temperature of 25 °C with a shaking speed of 80 rpm for up to 7 days. The batch experiments were done in triplicates to ensure that the differences observed were statistically significant. After the predetermined shaking time, pH of the suspensions were measured and the liquid portion was collected by filtration through 0.2 µm syringe driven-type membrane filters (Sartorius AG, Germany). The concentrations of dissolved Fe, S and Al were measured by ICP-AES while the solid portion was washed with deionized water, dried in a vacuum drying oven at 40 °C for 24 hours prior to characterization.

3.3 Electrochemical studies

Electrochemical studies were conducted to investigate electrochemical dissolution of pyrite and the effects of selected metal oxides (hematite and alumina) on the half-cell reactions of this process. With electrochemical studies, the anodic and cathodic half-cell reactions can be separately controlled and elucidated, which was impossible with batch-type experiments. The setup for these experiments was a conventional three-electrode configuration consisting of a reference electrode (Ag|AgCl electrode in saturated KCl, +0.197 V vs. SHE), a counter electrode (Pt) and a working electrode (pyrite), which are connected to SI 128B electrochemical measurement unit (Solartron Instruments, UK). The working temperature of this system was maintained at 25 °C using a constant low temperature water bath recirculating system (BB400, Yamato Scientific Co Ltd., Japan). For the electrolyte used in the experiments, 0.1 M Na_2SO_4 was selected as supporting electrolyte. Figure 3-7 illustrates a schematic diagram of the electrochemical setup used in this study.

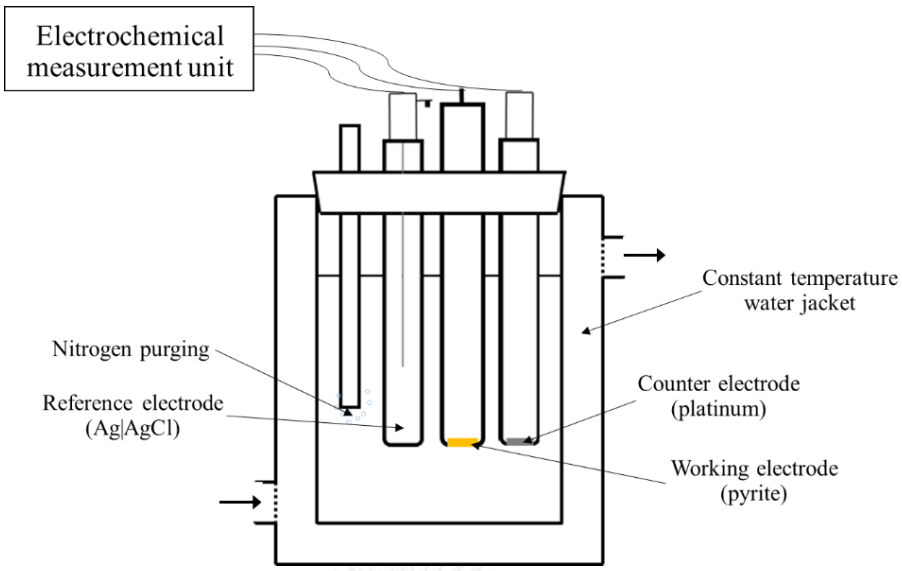

Figure 3-7 Schematic diagram of electrochemical experimental setup

For the preparation of the pyrite electrode, a pyrite crystal was cut into a cuboid, connected to copper wires with silver conducting paste and fixed inside a plastic pipe with Technovit®3040 nonconductive resin (Heraeus Kulzer GmbH, Germany). The pyrite surface was then exposed by polishing with a series of Si-carbide papers (#240, #600 and #1000). Before each measurement, the pyrite electrode was polished with Si-carbide papers (#1200 and #1500), fine polished with alumina suspensions (5 μm and 1 μm) on a smooth glass plate and then ultrasonically cleaned for 5 minutes to obtain a fresh surface for the measurements. After each electrochemical experiments, the exposed surface area of pyrite electrode was measured by a digital microscope to obtain the working electrode's effective area for calculation of the current density. Figure 3-8 illustrates components of pyrite working electrode and Ag|AgCl reference electrode.

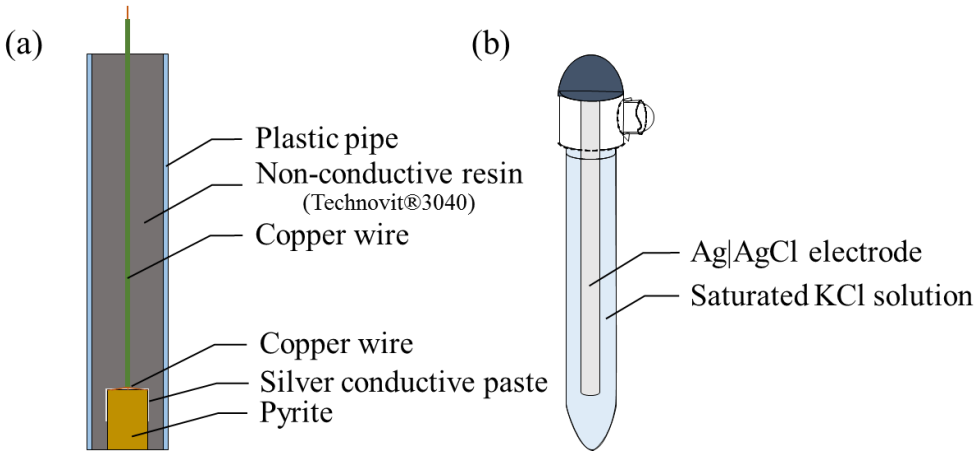

Figure 3-8 Schematic of cross-section of pyrite electrode (a) and schematic diagram of Ag|AgCl reference electrode (b)

Cyclic voltammetry (CV) experiments were conducted to investigate redox reactions at the pyrite working electrode's surface by observing current generated (moves of electrons) at different applied potentials. Meanwhile, chronoamperometry experiments were done to investigate the changes over time on each half-cell reactions at fixed potential. Both CV and chronoamperometry measurements were done after pretreatment of the pyrite electrode, which exposure of the electrode for oxidizing conditions for 24 hours to air (1), deionized water (2), 20 mg/l hematite suspension (3), 200 mg/l hematite suspension (4) or 200 mg/l alumina suspension (5).

Cyclic voltammetry measurements were done under anoxic condition in order to remove the interference caused by O_2. Prior to each experiment, the supporting electrolyte was equilibrated at 25 °C for at least 40 minutes, followed by N_2 gas purging without the working electrode for 20 minutes to remove dissolved O_2. After this, the "treated" working electrode was introduced into the system and re-purged for another 10 minutes. All cyclic voltammetry measurements started after stabilization of the electrode to its open circuit potential (OCP). The sweep direction was towards positive (anodic) potentials with a constant sweep rate. The measurements continued until +0.8 V vs reference (Ag|AgCl electrode) was reached. After this, the scan direction was reversed towards negative potentials (cathodic sweep) until -0.8 V vs Ag|AgCl, after which, the direction was changed back toward positive potential until the OCP. This constitutes 1 cycle of the CV measurements. In this study, 5 cycles of cyclic voltammetry measurements were recorded each experiment.

Potential sweep rate for the CV experiments with pyrite working electrode was determined by preliminary experiment, which vary the sweep rate from 5 mV/s to 120 mV/s as illustrated in figure 3-9. The results indicate increases in observed current density with faster sweep rate. In the CV study on pyrite electrode, the electrode reactions are reversible electrochemical adsorption/desorption on the surface with the sweep rate more than 30 mV/s. Therefore, the potential sweep rate of 30 mV/s was chosen as the profile of the result is clear and pyrite oxidation process can be easily observed (Kelsall, Yin, Vaughan, England, & Brandon, 1999).

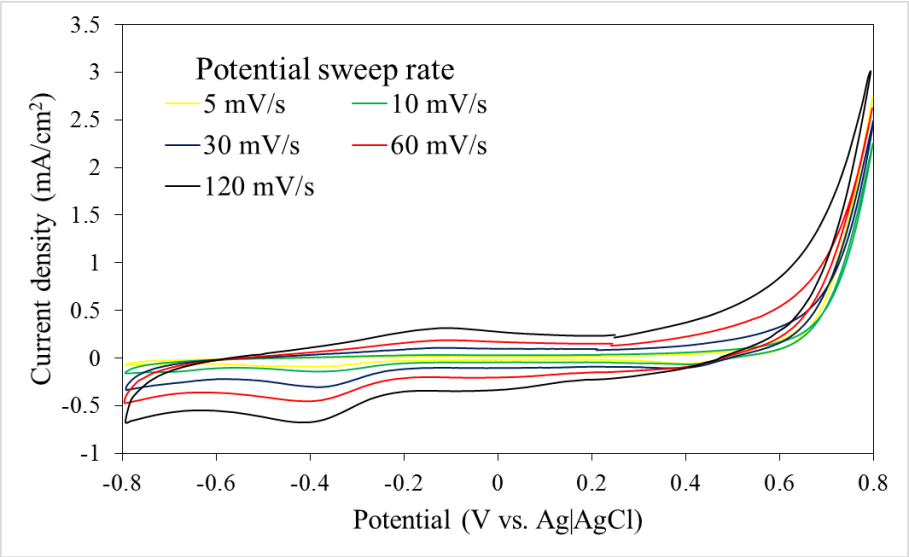

Figure 3-9 Cyclic voltammogram of polished pyrite at different sweep rate (2nd cycle; 25 °C; anoxic condition; no agitation)

3.4 Characterization of the oxidation layer on pyrite during its dissolution

The extent of pyrite dissolution is strongly influenced by the nature of the oxidation layer that is inevitably formed on the surface of pyrite. To investigate this layer, optical microscopy (VHS-1000 digital microscope, Keyence Corporation, Japan), scanning electron microscopy with energy dispersive spectroscopy capabilities (SEM-EDX)(SSX-550, Shimadzu Corporation, Japan) and diffuse reflectance Fourier transform infrared spectroscopy (DRIFTS) (FT/IR-6200HFV with DR PR0410-M attachment, Jasco Analytical Instruments, USA). For the DRIFTS analysis, the samples after the leaching experiments including the newly washed pyrite were crushed further to less than 50 µm.

CHAPTER 4
EFFECTS OF METAL OXIDES ON PYRITE DISSOLUTION

4.1 Nature of the oxidation layer formed during pyrite dissolution

DRIFTS spectra of fresh pyrite and pyrite oxidized in air for 3 and 7 days are shown in Figure 4-1. The strongest absorption band in all cases at 443.5 cm^{-1} is assigned to the S-S stretching of disulfide in pyrite (Evangelou, 1995). Higher absorption bands were observed after longer oxidizing time (after 3 and 7 days) inferred that oxidization products of pyrite were formed and accumulated on the surface with time. There were evidences of common oxidation products of pyrite, which are assigned to sulfate and its association with Fe^{3+} in the absorption range of 900-1200 cm^{-1} and sulfoxy anions (*e.g.*, SO_3^{2-}, $S_2O_3^{2-}$, $S_nO_6^{2-}$) around absorption band of 600-800 cm^{-1} (Egiebor & Oni, 2007).

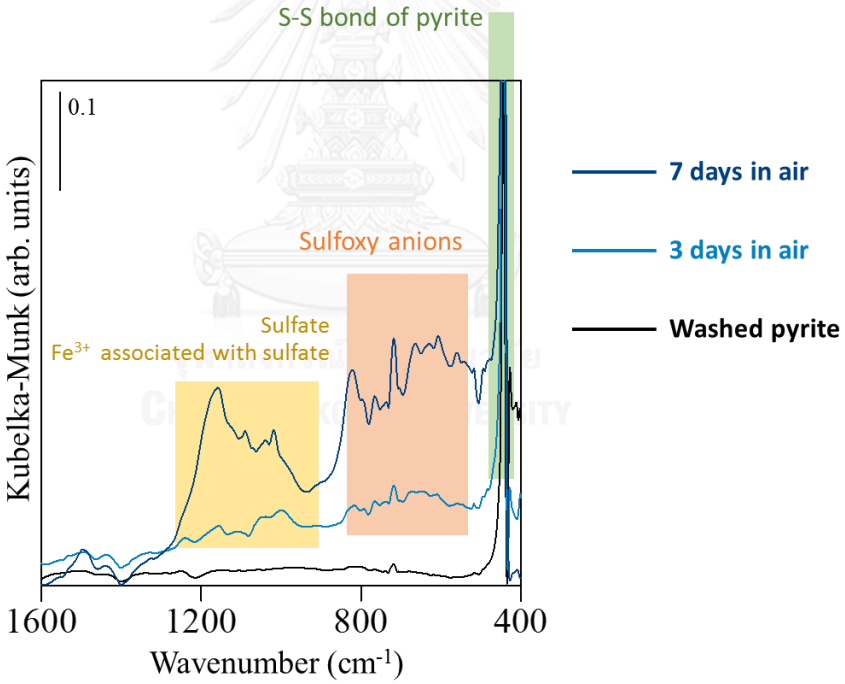

Figure 4-1 DRIFTS spectra of washed pyrite and pyrite oxidized in air for 3 and 7 days

Figure 4-2 summarize the changes over time of pH, Eh and concentration of dissolved S and Fe in mM (mmol/l) unit measured after shaking 1 g of washed pyrite in deionized water for up to 7 days. In this study, the extent of pyrite dissolution was evaluated from the dissolved S concentration because sulfur species are generally conservative ions and is one of the main products of the process as previously illustrated in Equations (2-4) and (2-5). As shaking time increased, pH of the solution gradually

decreased because acidity (H^+) was generated from pyrite dissolution (Figure 4-2a). Figure 4-2c shows increases in dissolved S concentration over time and then stabilized after 3 days, which indicates that apparent equilibrium was reached after about 3 days. In contrast, the concentration of dissolved Fe (Figure 4-2d) was lower than dissolved S by more than 10 times in terms of molar scale concentration. Theoretically, as Fe is also one of the main products of the process, the amount of leached Fe should only differ from that of S by ca. 2 times. This discrepancy could be attributed to the hydrolysis and precipitation of Fe^{3+} as $Fe(OH)_3$ under the pH condition of the experiments (pH > 3.5).

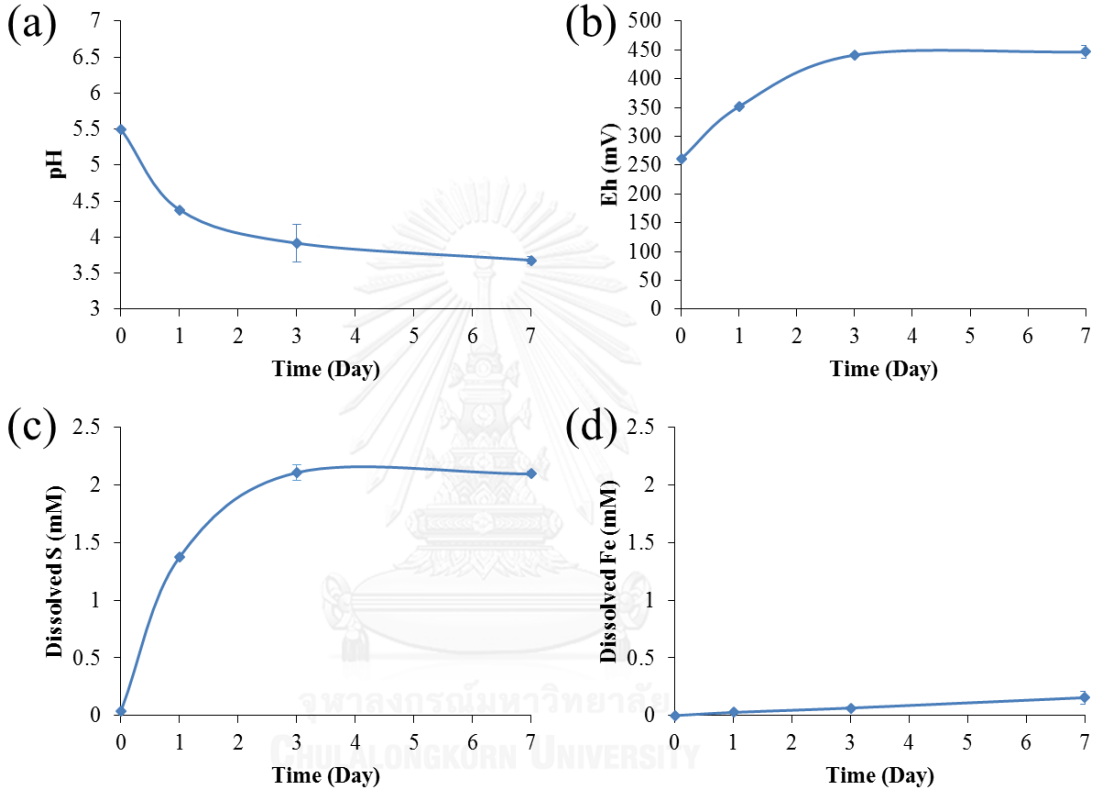

Figure 4-2 Changes of pH, Eh, and concentrations of dissolved S and Fe with time in batch experiment: (a) pH change with time, (b) Eh change with time, (c) dissolved S concentration in mM change with time, and (d) dissolved Fe concentration in mM change with time

Cyclic voltammetry measures the electrons generated by redox reactions on the surface of the working electrode under shifting applied potential. Figure 4-3 illustrates typical CV curve of polished pyrite in this study. During the anodic sweep (*i.e.*, towards positive potential), the working electrode is forced to behave as an anode and oxidation reactions are induced. In the anode, S^{2-} of pyrite is oxidized to produce sulfoxy anions and finally sulfate. Because the irreversible oxidation of pyrite starts around +0.5 V vs SCE (ca. 0.45 V vs Ag|AgCl) (Mishra & Osseo-Asare, 1988), the sharp rise in current density above this potential could be attributed to the oxidation of S^{2-} and that of Fe^{2+} to Fe^{3+}. Two main peaks in the cathodic scan (toward negative potential) at +0.4 and -0.4 V are attributed to the reduction of Fe^{3+} to Fe^{2+} and oxidation products formed during the previous anodic sweep, respectively.

In this study, pyrite working electrode was treated in different oxidizing conditions for 24 hours (1 day) prior to the measurement to obtain insights on the electrochemical properties of oxidation products formed on pyrite surface during the treatment. The differences in current densities between polished pyrite electrode and those treated reflect differences in their surface condition and properties of oxidation products formed on the surface. Figure 4-3 illustrates cyclic voltammogram of polished pyrite and those oxidized in air and deionized water for 24 hours. The result shows that CV of polished pyrite electrode yielded the highest current density during the anodic sweep compared to the other cases. This means that polished pyrite electrode is very reactive compared to those treated in air and DI water. This high reactivity on freshly polished pyrite surface is attributed to the structural sulfur vacancy and defects (i.e. broken S-S bonds) produced during the polishing process. The Fe and S atom around defects are more reactive to water molecules compared with an ideal non-defective surface (Nair, Schreiner, & Marx, 2006). For the oxidation products of pyrite formed during the treatment in air and DI water for 24 hours, the result shows current density profile in anoxic condition of the pyrite oxidized in air was higher compared with that in DI water (Figure 4-3). On the other hand, Tabelin et. al. (2016) performed similar experiments with pyrite treated in air and DI water for 15 hours under oxic condition (Figure 4-4). Their results show higher observed current density in the case of pyrite treated in DI water instead. The difference is most probably due to the existence of dissolved oxygen in the electrolyte during the measurement.

A studied oxidation of {(100) surface of pyrite in the presence of O_2 gas, H_2O gas and their mixtures. They found that pyrite oxidation was undetectable in pure H_2O gas system (absence of O_2) and pyrite only shows small degree of oxidation with pure O_2 gas. They also found that pyrite surface was aggressively oxidized in the O_2-H_2O gas mixture with critical molar ratio of 1:1 (Rosso, Becker, & Hochella, 1999).

This phenomenon could help explain the cyclic voltammetry results (figure 4-3 and 4-4). These results infer that more oxidation products were accumulated on the pyrite surface after 1 day treatment in DI water. Under anoxic condition (Figure 4-3), that is without the presence of dissolved O_2 in the electrolyte, the oxidation of partly oxidized species of the oxidized layer on pyrite surface become more difficult and results in lower current density measured in the case of pyrite treated in DI water. In oxic condition (Figure 4-4), with presence of dissolved O_2 in the electrolyte, the oxidation proceeds more easily so higher current densities were measured in the case of pyrite treated in DI water as it initially had more oxidation products on the surface during the pretreatment.

As the sweep direction is reversed during the cathodic sweep, the observed current density is the mainly reduction of Fe^{3+} to Fe^{2+} and reduction of the oxidation products formed during the anodic sweep. The results in figure 4-3 shows that more reductive current (more negative value) was observed in the case of polished pyrite consistent with relatively higher amounts of oxidation products formed during the previous anodic sweep. The cathodic scan in oxic condition (Figure 4-4) could also be explained in the same way.

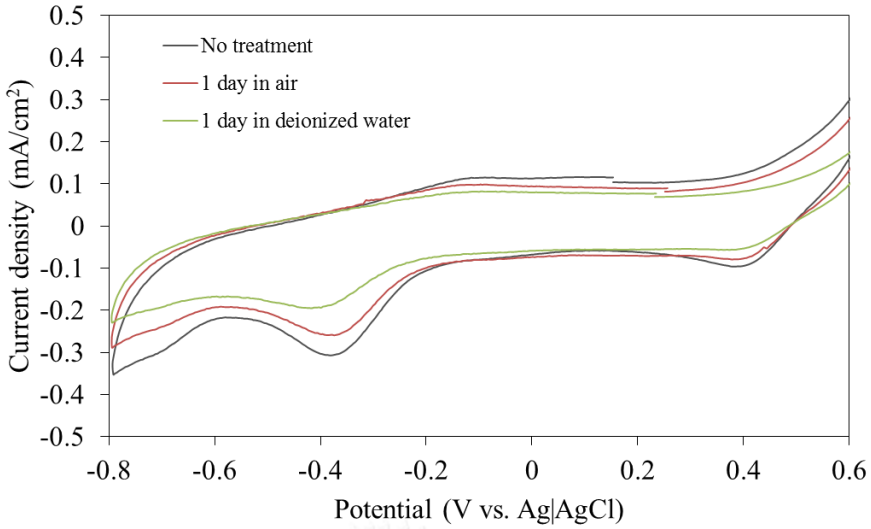

Figure 4-3 Cyclic voltammogram of polished pyrite and pyrite exposed to air and DI water for 24 hours (2nd cycle; Sweep rate 30 mV/s; 25 °C; anoxic condition; no agitation)

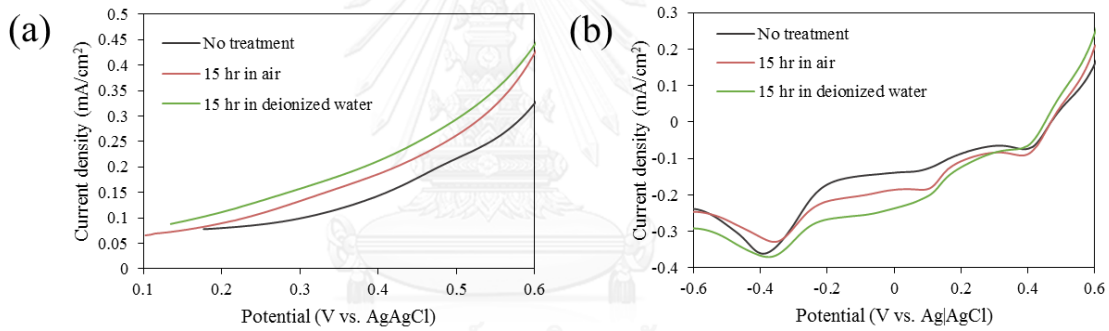

Figure 4-4 Cyclic voltammogram of polished pyrite and pyrite exposed to air and DI water for 15 hours; (a) anodic sweep, and (b) cathodic sweep (Sweep rate 30 mV/s; 25 °C; oxic condition; no agitation) Figure redrawn and adapted from Tabelin et. al. (2016)

Chronoamperometry experiments were conducted to observe the effects of the oxidation products on each of the half-cell reactions over time. Anodic polarization of pyrite was done at a potential of +0.6 V vs Ag|AgCl under anoxic condition. This potential was chosen because pyrite oxidation becomes irreversible after +0.5 V vs SCE (ca. 0.45 V vs Ag|AgCl) (Mishra & Osseo-Asare, 1988) and the anodic reaction of pyrite oxidation doesn't involve O_2 as shown in Equation (2-3). On the other hand, cathodic polarization was done at -0.2 V vs Ag|AgCl under oxic condition because at this potential, reductive dissolution of pyrite doesn't occur (Kelsall et al., 1999) and O_2 is a crucial reactant as described in Equation (2-1). During chronoamperometry, the electrolyte was continuously agitated at 250 rpm by a magnetic stirrer to ensure that reactants were continuously supplied to the pyrite surface.

Figure 4-5 illustrates anodic polarization profile of polished pyrite and those oxidized in air and DI water for 24 hours at the potential of +0.6 V vs Ag|AgCl. The observed current density indicates oxidation reactions on the surface of the pyrite

working electrode, which can be mainly attributed to the oxidation of very reactive defects on polished pyrite, sulfoxy anions to sulfate, Fe^{2+} to Fe^{3+} and dissolution of pyrite itself. With time, the measured current density gradually decreased and results in 3 different regions with different characteristics. The first region lasted for a very short period in the beginning of the measurement as emphasized in figure 4-6. In this region, very high current densities with very steep slope profiles were observed, indicating that every kind of reactions mentioned above make up this current. The most important reaction in this region, accounted for the steep profile, is the oxidation of highly reactive defects (*i.e.* steps, kinks, and sulfur vacancies) as the result implies highest amount of these reactive defects in the case of polished pyrite to the lower in those oxidized in air and DI water respectively. This is also consistent with the previous interpretation of the CV result (Figure 4-3 and 4-4) as explained earlier as the degree of oxidation during 24 hours treatment time is more extensive in DI water than in air and polished pyrite. The second region is described as gradually decreasing in current density before the current density profile reached apparent equilibrium and accounting for the oxidation of sulfoxy anions to sulfate, Fe^{2+} to Fe^{3+} and the dissolution of the pyrite crystal. The gradual decrease in this region is corresponding to the oxidation of sulfoxy anions to form sulfate as this process comprises several elementary steps before the final product could be formed. The final region is where the observed current density reached apparent equilibrium. The anodic currents corresponding for this region are dissolution of pyrite crystal and oxidation of Fe^{2+} to Fe^{3+}.

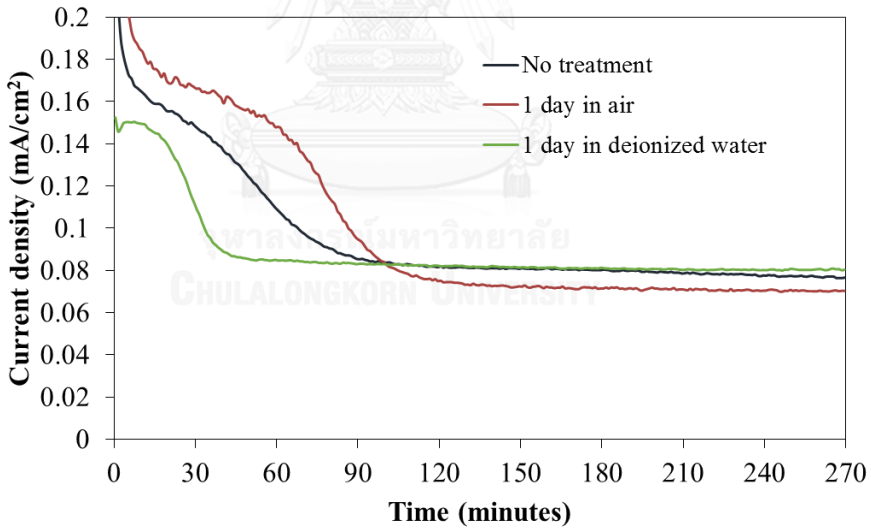

Figure 4-5 Anodic polarization of polished pyrite and pyrite exposed to air and DI water for 24 hours (Potential +0.6 V vs Ag|AgCl; 25 °C; anoxic condition; 250 rpm agitation)

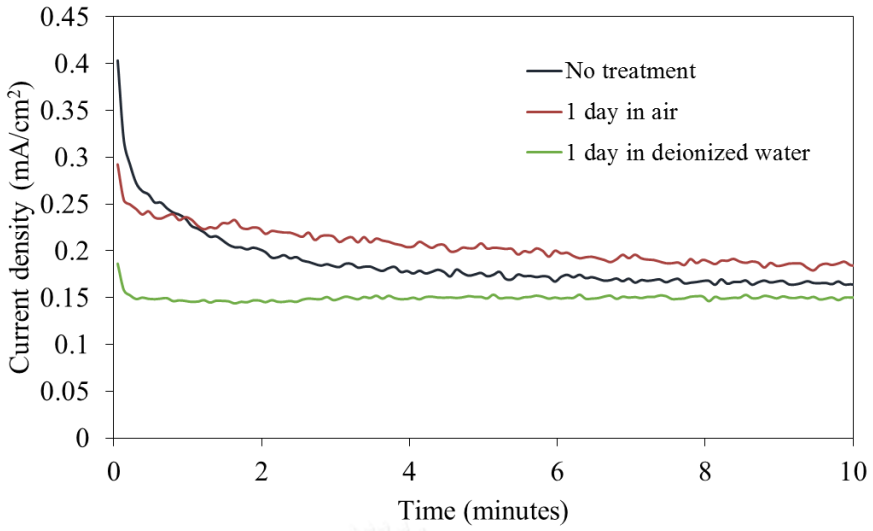

Figure 4-6 First 10 minutes of anodic polarization of polished pyrite and pyrite exposed to air and DI water for 24 hours (Potential +0.6 V vs Ag|AgCl; 25 °C; anoxic condition; 250 rpm agitation)

To confirm the significance of dissolved O_2 in the cathodic half-cell reaction, cathodic polarization measurements were done in anoxic (without O_2) and oxic (with O_2) condition. The result (figure 4-7) suggests that without dissolved O_2 in the electrolyte, the cathodic half-cell reaction of pyrite was drastically lower as there were no oxidants (e.g. Fe^{3+} or O_2) available in the electrolyte.

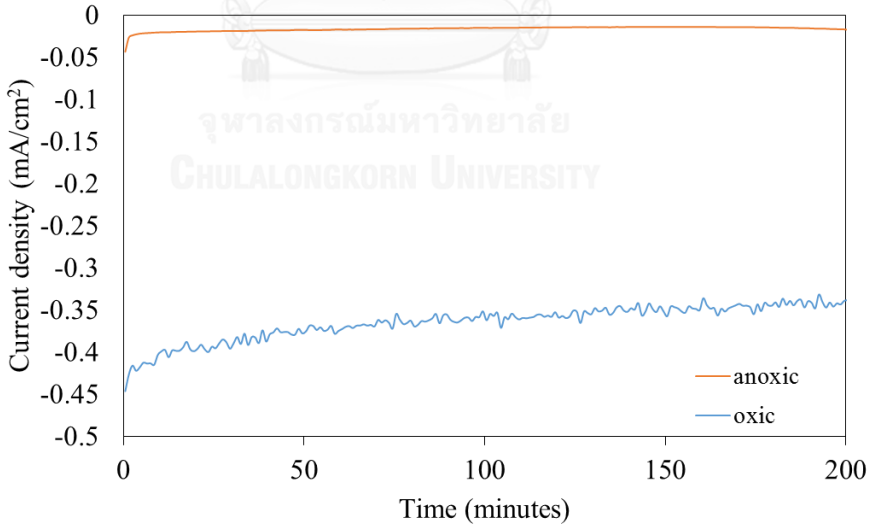

Figure 4-7 Cathodic polarization of polished pyrite in oxic and anoxic condition at pH 2.0 (Potential -0.2 V vs Ag|AgCl; 25 °C; 250 rpm agitation)

Figure 4-8 illustrates cathodic polarization profile of polished pyrite and those treated in air and DI water for 24 hours at the potential of -0.2 V vs Ag|AgCl. The observed current density, in this case, reflects reduction reactions on the surface of the pyrite working electrode (*i.e.* reduction of O_2 and Fe^{3+}). The result implies that polished

pyrite is reductively reactive compared to those treated in air and DI water based on more negative observed current density in the prior case. Similar to the anodic polarization of pyrite as discussed, highly reactive structural defects of pyrite (*i.e.* steps, kinks, and sulfur vacancies) can also undergo reductive reactions. This summarizes that the defect sites on pyrite could act as either anode or cathode, then degraded quickly due to their high reactivity. As another issue of interest, the shape of the current profile, which gradually increase and then decrease, could be the effects of dissolved O_2 in the electrolyte. As figure 4-7 suggested that the current density profile without dissolved O_2 in the system (anoxic condition) was almost linear with very low intensity of observed current.

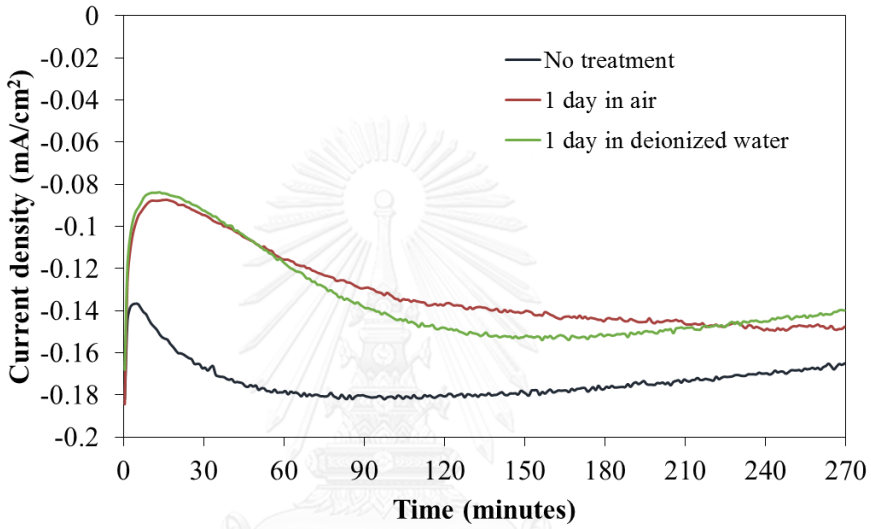

Figure 4-8 Cathodic polarization of polished pyrite and pyrite exposed to air and DI water for 24 hours (Potential -0.2 V vs Ag|AgCl; 25 °C; oxic condition; 250 rpm agitation)

4.2 Effects of hematite on pyrite dissolution

4.2.1 Interactions of pyrite with hematite suspension

3D photomicrographs of the pyrite exposed to the hematite suspension show that hematite particles are attracted to pyrite largely because of their oppositely charged surfaces (Figure 4-9). The presence of attached hematite particles on pyrite surface were also supported by SEM-EDX of pyrite after 7 days of shaking in hematite suspension (Figure 4-10). SEM microscopic image at magnification scale of 8,000 times (Figure 4-10b) illustrates hematite particle (α-Fe_2O_3) attached on pyrite surface as deduced from the stronger signals of O and Fe (Figire 4-10c and 4-10d) in the same position of the attached particle compared to background signals of pyrite (FeS_2). The elemental mapping of S also confirmed that sulfur was not presented in the particle. Note that the negative signal in the lower-left area of the map of S was due to the "shadow" effect, that is, the hematite particle blocked the line of sight of the X-ray beams.

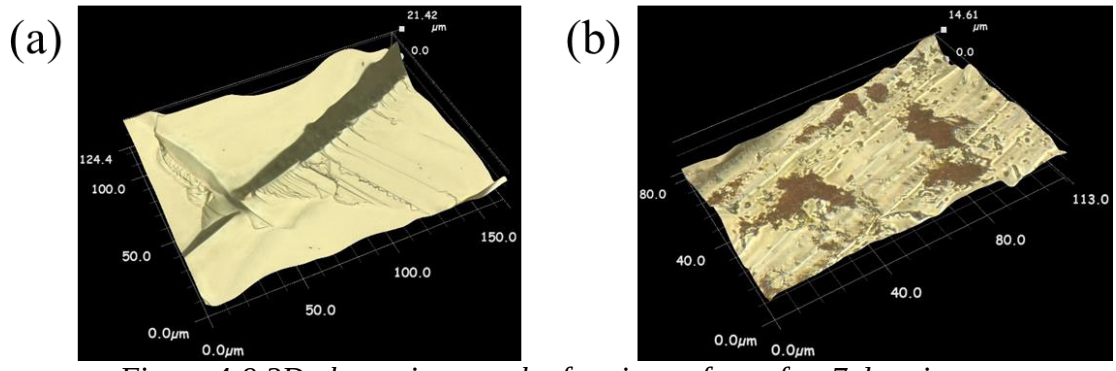

Figure 4-9 3D photomicrograph of pyrite surface after 7 days in (a) deionized water, and (b) 200 mg/l hematite suspension

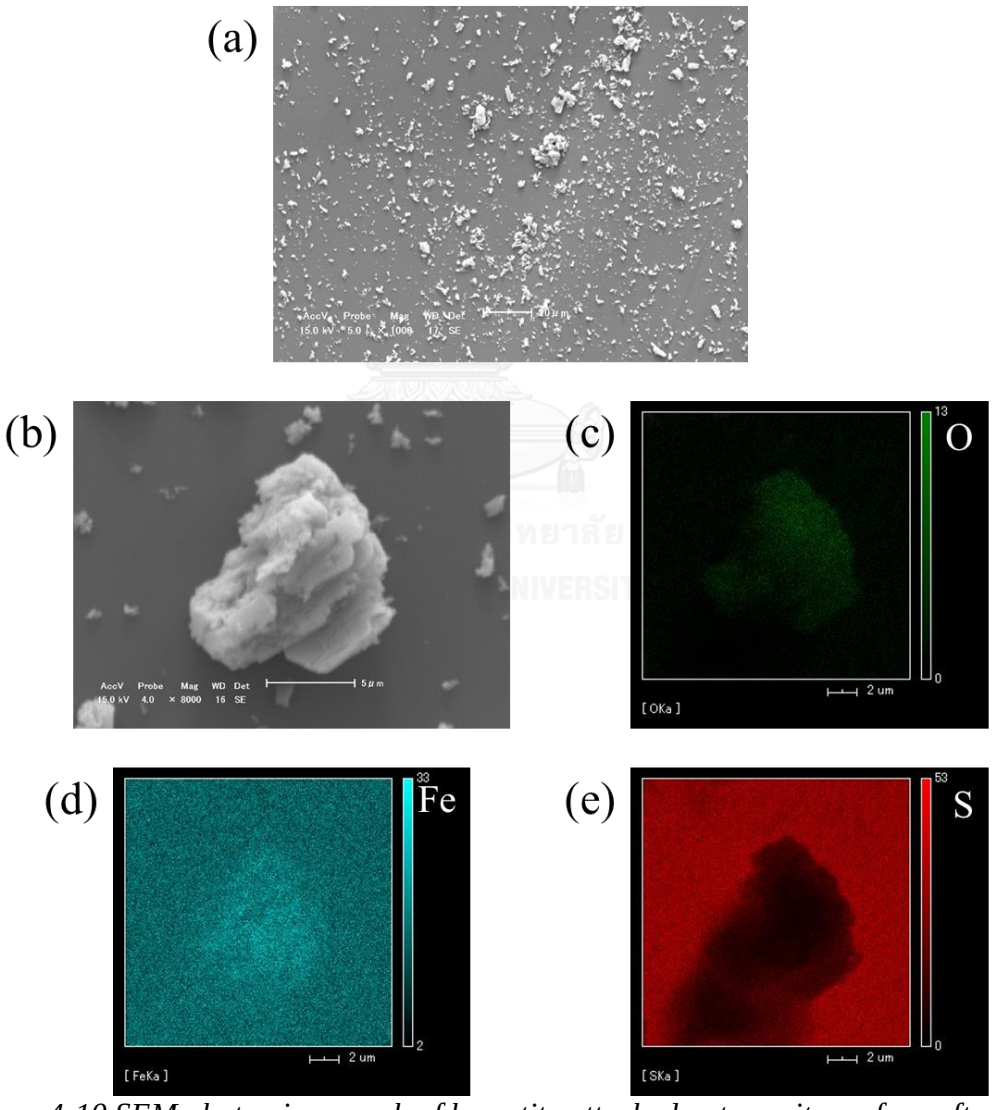

Figure 4-10 SEM photomicrograph of hematite attached onto pyrite surface after 7 days at (a) 1000x magnification scale, and (b) 8000x magnification scale with elemental maps of O (c), Fe (d), and S (e) of the particle

Batch-type experiment was conducted by shaking pyrite in deionized water as control and in 200 mg/l hematite suspension to evaluate the effects of hematite on the net oxidation of pyrite. In the experiments with DI water and hematite suspension, the measured pH, Eh and dissolved S shifted and reached "apparent equilibria" after 3 days. The results indicate that the pH and Eh value of the leachate during the first 7 days was not affected by the presence of hematite (Figure 4-11a and 4-11b) as the pH value gradually decreased with time while Eh value increased. The release of S, an indicator for assessing degree of pyrite oxidation, was substantially lowered in the presence of hematite, which implied that hematite somehow suppressed pyrite dissolution (Figure 4-11c). In comparison, there was no statistical significant change in dissolved Fe in the leachate (Figure 4-11d). The reason for this could be explained by the geochemical modelling calculation of pH-Eh diagram based on actual concentrations of Fe and S measured in the batch experiment with hematite suspension (Figure 4-13). Thermodynamics predicts that under the condition of the batch experiment, hematite could be dissolved in the pH and Eh condition even though hematite is considered as the most thermodynamically stable phase of iron oxide. As hematite in the suspension was slightly dissolved, it contributed to the total amount of dissolved Fe in the leachate along with Fe released from pyrite dissolution. This could explain the statistically similar dissolved Fe concentration despite the lower extent of pyrite dissolution in the presence of hematite. Note that in the case of hematite, the measured quantity of dissolved Fe compared with that of S is also far lower in term of molar concentration as pH plays important roles for controlling the concentration of dissolved Fe (Figure 4-12).

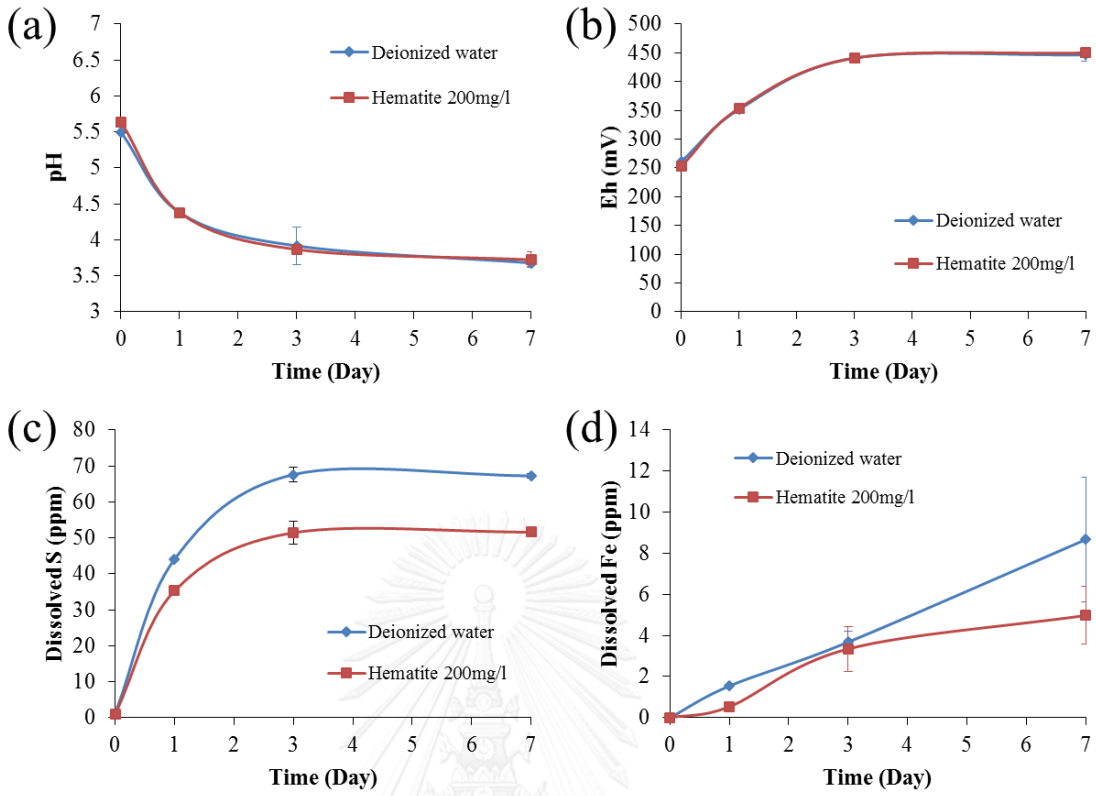

Figure 4-11 Changes of pH, Eh, and concentrations of dissolved S and Fe with time in deionized water and hematite suspension: (a) pH change with time, (b) Eh change with time, (c) dissolved S concentration in ppm change with time, and (d) dissolved Fe concentration in ppm change with time

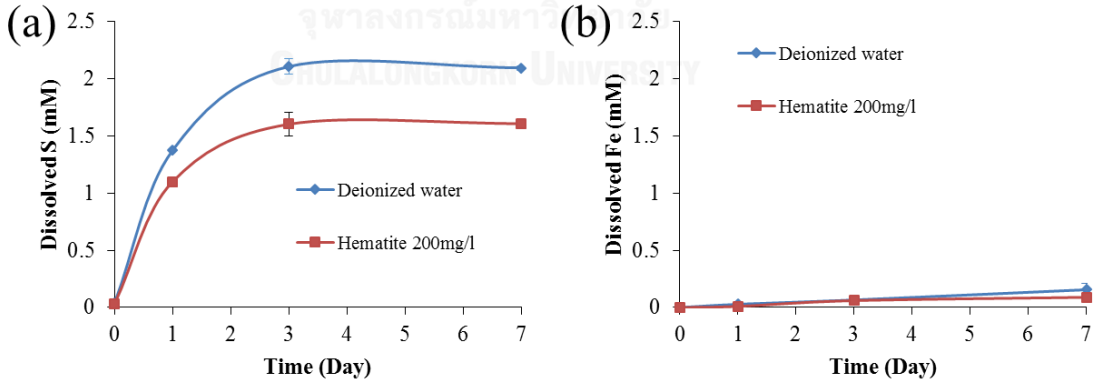

Figure 4-12 Changes of concentrations of dissolved S and Fe with time in deionized water and hematite suspension: (a) dissolved S concentration in mM change with time, and (b) dissolved Fe concentration in mM change with time

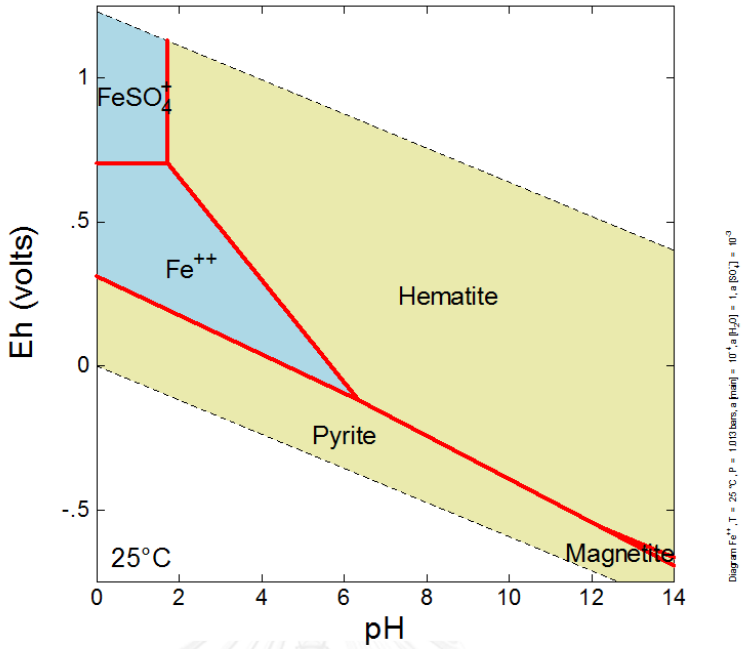

Figure 4-13 pH-Eh diagram of batch-type experiment with hematite (25 °C; activity of Fe = 10^{-4}; activity of S = 10^{-3})

DRIFTS spectra of fresh pyrite and those shaken in deionized water and hematite suspension for 7 days (Figure 4-14) were identified to gain information of oxidation products formed on pyrite surface in each case. The result of pyrite exposed to deionized water also indicates similar oxidation products of pyrite to the case of pyrite exposed to air (*i.e.* sulfoxy anions and sulfates) (Figure 4-1), which was explained in more detail earlier. With the presence of hematite, the absorption peaks of the oxidation products of pyrite become less prominent, which infer that comparatively lower amounts of the oxidized species formed on the surface during batch experiments.

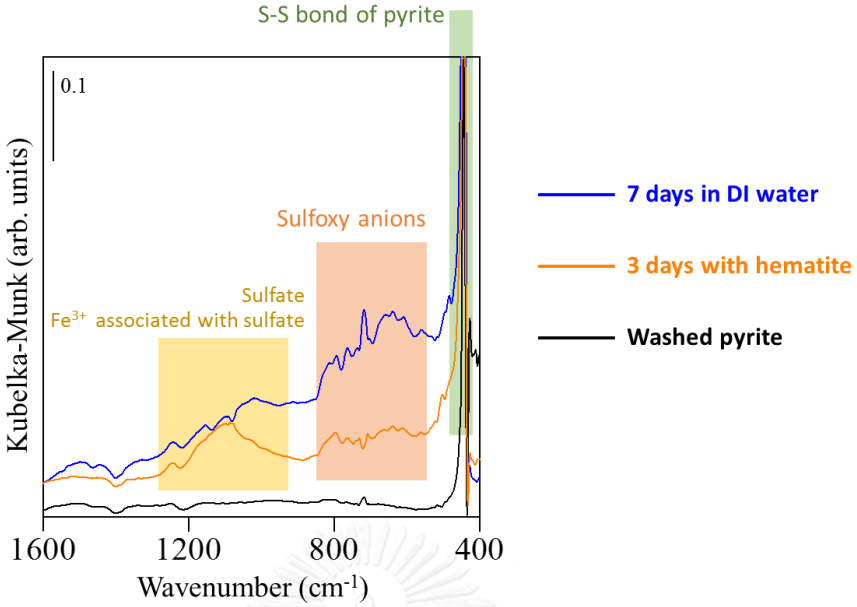

Figure 4-14 DRIFTS spectra of washed pyrite and pyrite after leaching for 7 days at 25 °C in hematite suspension and deionized water

In the next sub-section, the effects of hematite on pyrite dissolution will be further studied into greater detail using different electrochemical techniques, which can separately study the effects on each of the half-cell reaction of pyrite dissolution.

3.2.2 Electrochemical study of the effects of hematite on pyrite dissolution

Figure 4-15 illustrates cyclic voltammograms of polished pyrite and those oxidized in air, deionized water, 20 mg/l hematite suspension and 200 mg/l hematite suspension for 24 hours. In comparison to CV of pyrite treated in deionized water, higher anodic current density was observed on pyrite electrode treated in 200 mg/l hematite suspension. In contrast to the case of pyrite treated in 20mg/l hematite suspension, which show similar current density profile to that of the pyrite treated in deionized water. This suggest that the effects of hematite on the anodic and cathodic half-cell reactions during pyrite dissolution was insignificant if the amount of hematite attached onto pyrite was insufficient (*i.e.* in case of pyrite treated in 20 mg/l hematite suspension for 24 hours).

There are 2 possible explanations for the increase in current density with the presence of 200 mg/l hematite suspension compared to the case of deionized water. The first explanation is that hematite suppressed the dissolution, as illustrated by lower amounts of oxidation products formed on the pyrite surface (Figure 4-14) and also less degradation of the polishing defects (Figure 4-17). This resulted in higher observed current density as already explained earlier similar to figure 4-3 and 4-6. Another explanation is that hematite directly enhanced the anodic half-cell reaction of pyrite dissolution; the details of which will be explained with the anodic polarization of pyrite treated in hematite suspension (Figure 4-16).

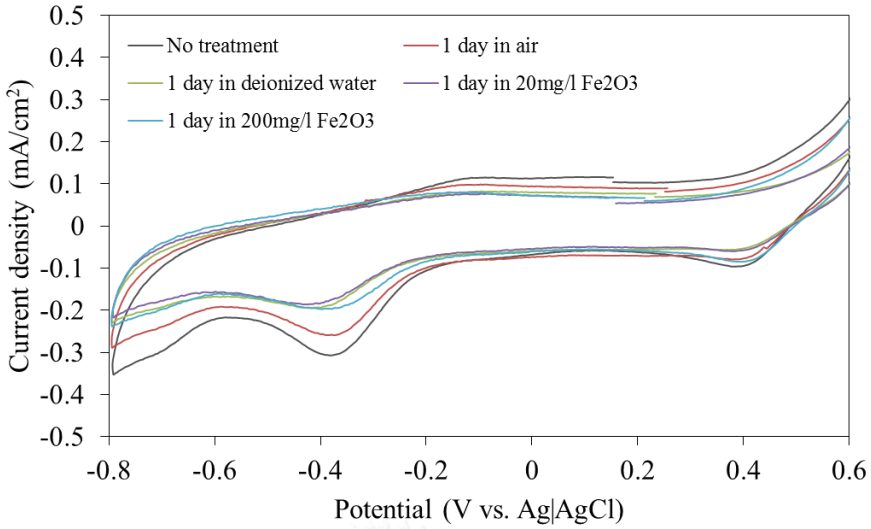

Figure 4-15 Cyclic voltammogram of polished pyrite and pyrite exposed to air, DI water and hematite suspensions for 24 hours (2nd cycle; Sweep rate 30 mV/s; 25 °C; anoxic condition; no agitation)

Anodic polarization current density profiles at fixed potential of +0.6 V vs Ag|AgCl of pyrite oxidized in 20 mg/l hematite suspension and 200 mg/l hematite suspension is shown in figure 4-16. Figure 4-17 confirms that oxidation of defects after 24 hours in 20 mg/l and 200 mg/l hematite suspensions compared to that of deionized water as deduced previously in the last paragraph. Figure 4-16 shows higher current densities measured in the case of pyrite treated in 200 mg/l hematite suspension for 24 hours, which could be the result of enhancement of the anodic half-cell reaction of pyrite dissolution by the presence of hematite. As hematite is also a semiconductor like pyrite, its attachment onto pyrite probably enhanced the overall dissolution of pyrite by acting as "electron-bridge", an effect that allows electron to be transferred easier between anodic sites localized around S_2^- and cathodic sites localized around Fe^{2+} in the structure of pyrite surface. The reason for hematite to have the effect on pyrite could be due to the interaction between Fe^{3+} in hematite and pyrite as it is well-documented that many forms of Fe^{3+} adsorbed on pyrite can enhances its dissolution (add references here).

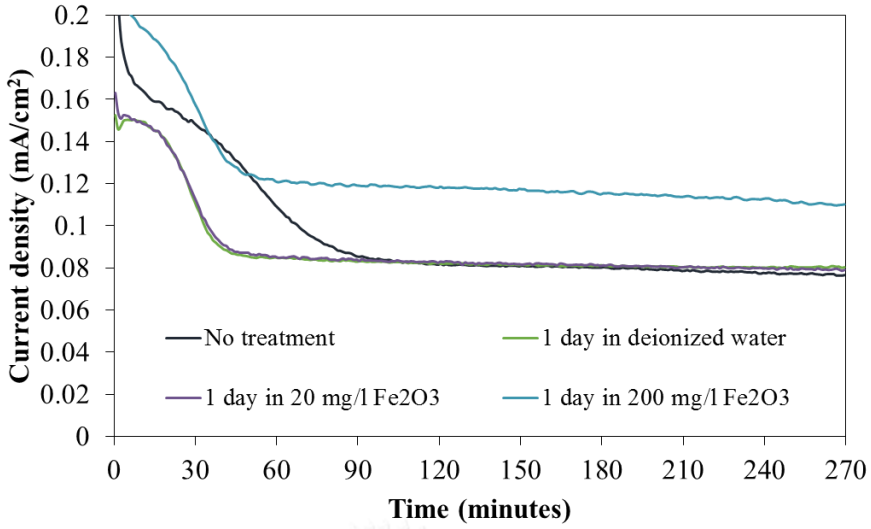

Figure 4-16 Anodic polarization of polished pyrite and pyrite exposed to DI water and hematite suspensions for 24 hours (Potential +0.6 V vs Ag|AgCl; 25 °C; anoxic condition; 250 rpm agitation)

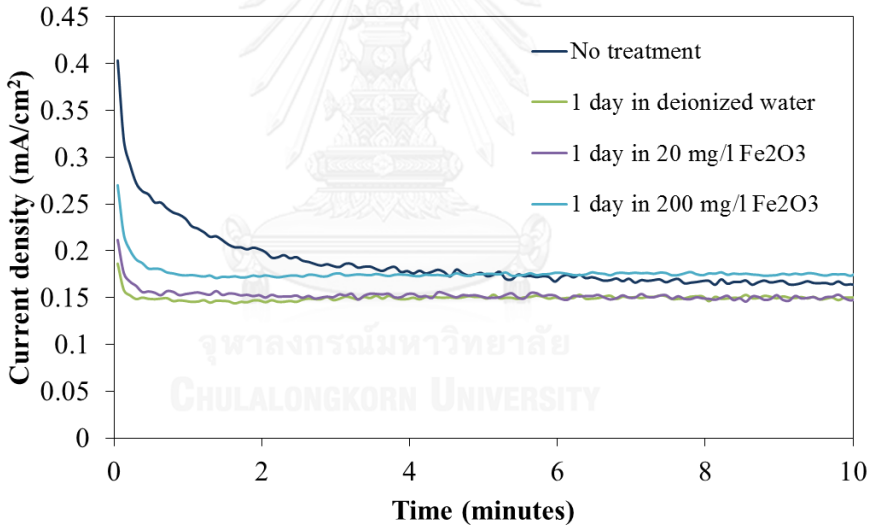

Figure 4-17 First 10 minutes of anodic polarization of polished pyrite and pyrite exposed to DI water and hematite suspensions for 24 hours (Potential +0.6 V vs Ag|AgCl; 25 °C; anoxic condition; 250 rpm agitation)

Figure 4-18 illustrates cathodic polarization profile of pyrite oxidized in 20 mg/l hematite suspension and 200 mg/l hematite suspension for 24 hours at the potential of -0.2 V vs Ag|AgCl. The result shows sign of decreases in intensity of current density with higher amount of hematite on pyrite surface. The reason for this might be because hematite attached on pyrite surface physically "protect" pyrite from oxidants (i.e. O_2 and Fe^{3+}), which is the main source of cathodic current in the measurement. As for the effect of hematite particle concentration in the 24 hours treatment (20 mg/l and 200 mg/l), higher amount of hematite showed more suppression in current density as the lowest measured current density profile was accounted from the case with 200 mg/l

hematite particle, followed by the case of 20 mg/l hematite particle suspension and deionized water (control case) respectively.

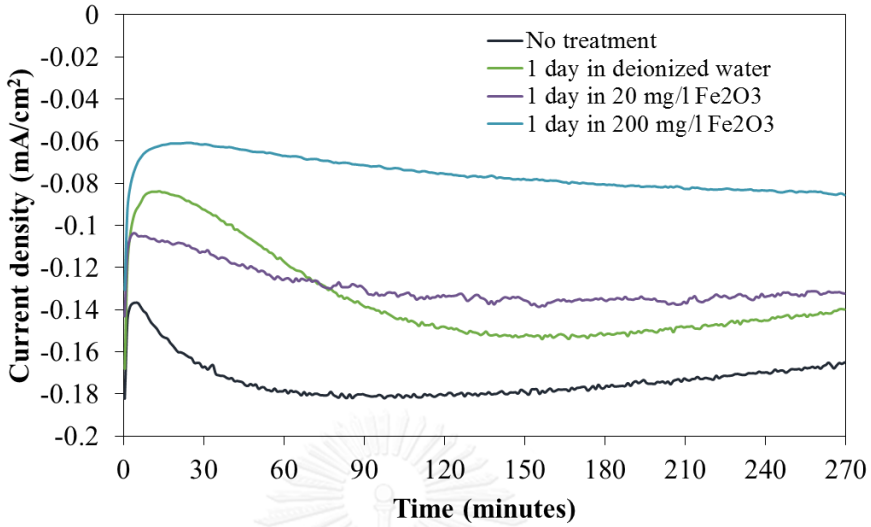

Figure 4-18 Cathodic polarization of polished pyrite and pyrite exposed to air, DI water and hematite suspensions for 24 hours (Potential -0.2 V vs Ag|AgCl; 25 °C; oxic condition; 250 rpm agitation)

4.3 Effects of alumina on pyrite dissolution

4.3.1 Interactions of pyrite with alumina suspension

In contrast to fresh pyrite surface, which is negatively charged over the measurement, alumina has a negative charge at pH less than ca. 8 similar to hematite. This charge difference verifies the possibility of attachment of particles onto pyrite surface as confirmed by 3D microscopic images of pyrite surface after 7 days in DI water or 200 mg/l alumina suspension (Figure 4-19). For the identification of those attached particle, the identical particle group was examined by SEM-EDX and elemental mapping of Al, O, Fe and S (Figure 4-20). According to the elemental maps, the composition of the attached particles was mainly Al (Figure 4-20b) and O (Figure 4-20c) while the background of the SEM image (Figure 4-20a) is identified as pyrite demonstrated by elemental maps of Fe (Figure 4-20d) and S (Figure 4-20e). There is also undetectable signal of Fe and S in the area supposed to be pyrite located at the lower left area of the micrograph. The effect is probably because of the “shadow” effect similar to that shown in figure 4-10. The testimony of overshadowing can also be further confirmed by the color contour mapping of the particle in 3D microscopic image (Figure 4-19b).

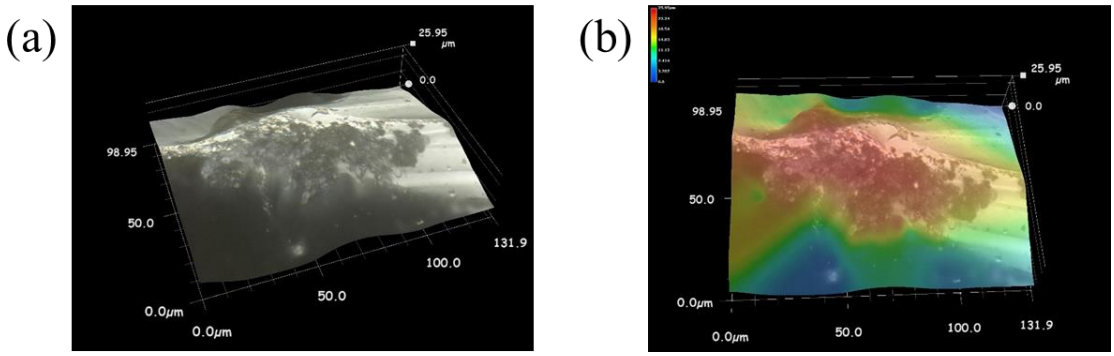

Figure 4-19 3D photomicrograph of pyrite surface after 7 days in 200 mg/l alumina suspension (a) and its contour color mapping (b)

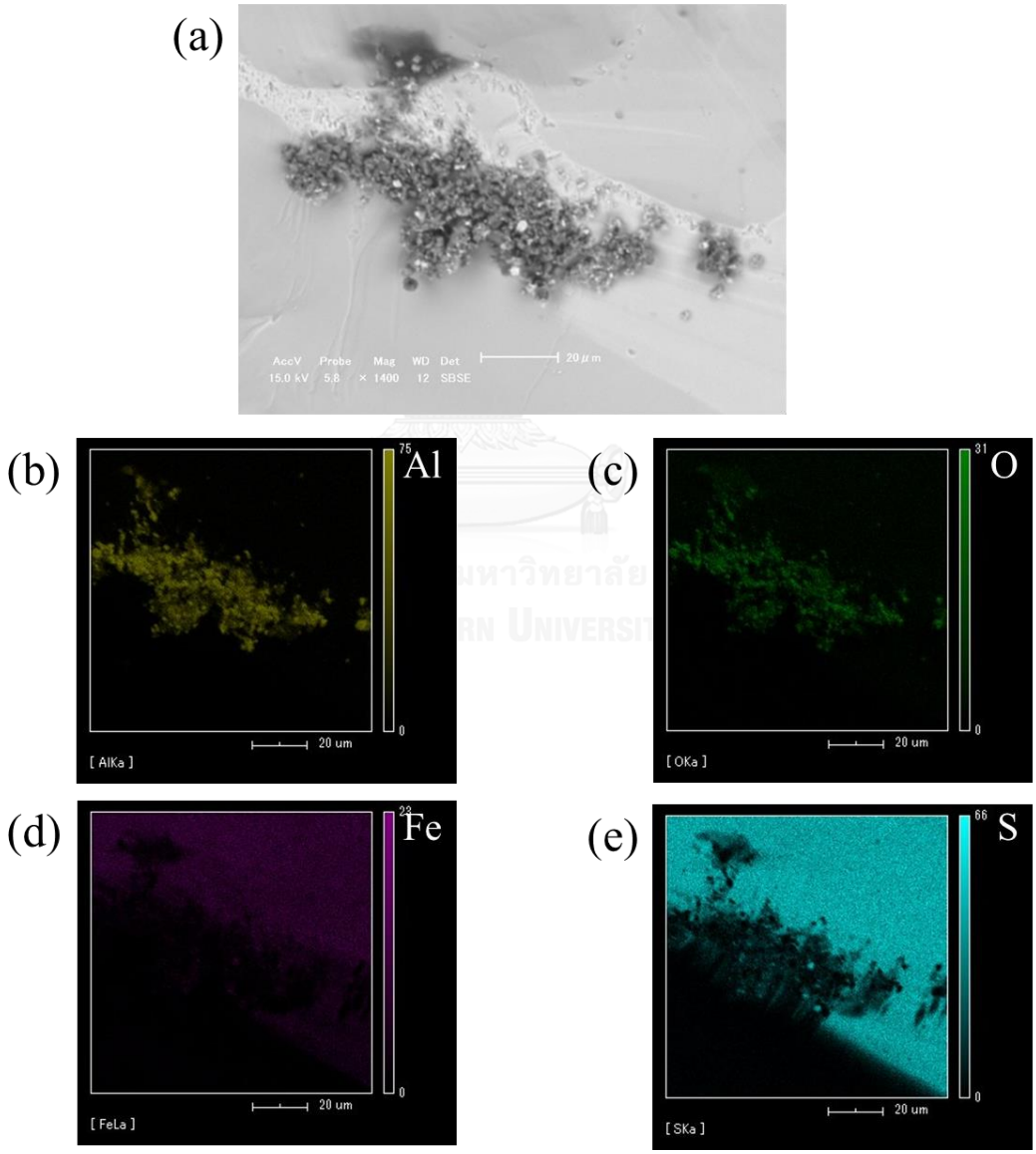

Figure 4-20 SEM photomicrograph of alumina attached onto pyrite surface after 7 days at with elemental maps of Al(b), O (c), Fe (d), and S (e) of the particle

To further verify the statement, numerous point analyses were done in the same area of interest as the measurement locations are notified by points in figure 4-21. There are 3 district regions of interest classified by the colour of points as blue, orange and green. It is important to note that elemental analysis using SEM-EDX is a semi-quantitative technique, which the data regarding quantity of each element can be used in comparative purposes and should not be regarded as the same level of confidence as other quantitative techniques (*i.e.* ICP-AES or XRF). For the results of point analysis, the area deduced to be responsible for alumina particles attached on pyrite shows high amount of Al and O, with noticeably amount of Fe and S signals solidified the statement that this locality belongs to alumina particles attached onto pyrite. The orange point was chosen as a representative of the area deduced to be pyrite as the background of the SEM image. As predicted, the signals found in the region are strong positive signal of Fe and S with the molar ratio of the measured semi-quantitative result to be ca. 2 corresponding to pyrite (FeS_2). On the other hand, the black pitch denoted as green point indicates rather high intensity of Fe and S signals along with positive signals of other elements such as O, Na and Al. Without any concrete prove, black pitch area might belongs to the concentrated impurity within pyrite crystal.

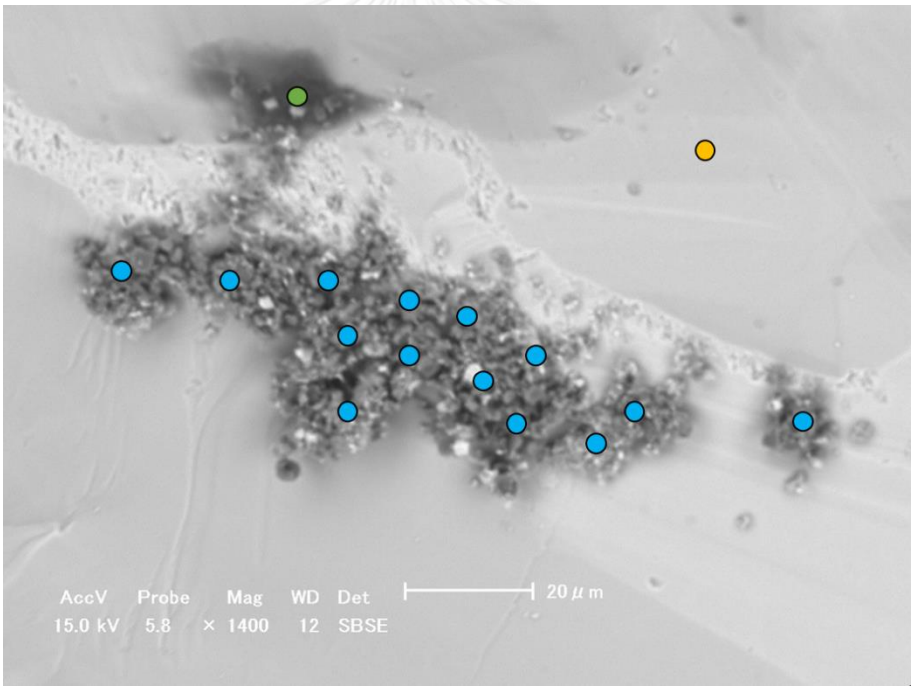

Figure 4-21 Targets for point analysis of SEM photomicrograph of alumina attached onto pyrite surface after 7 days

Figure 4-22 illustrates SEM image and elemental mapping of alumina particle on pyrite after 7 days of shaking in alumina suspension. The particle is deduced to be alumina (α-Al_2O_3) based on strong signals of Al (Figure 4-22b) and O (Figure 4-22c) in the same region as the particle. The elemental maps of Fe (Figure 4-22d) and S (Figure 4-22e) also support the statement as Fe and S signals are not presence at the alumina particle. The background of the image is also identified as the surface of pyrite from prominent signals of Fe and S. In this case as well, the dark area in the lower left part of the S map is caused by the "shadow" effect of the particle.

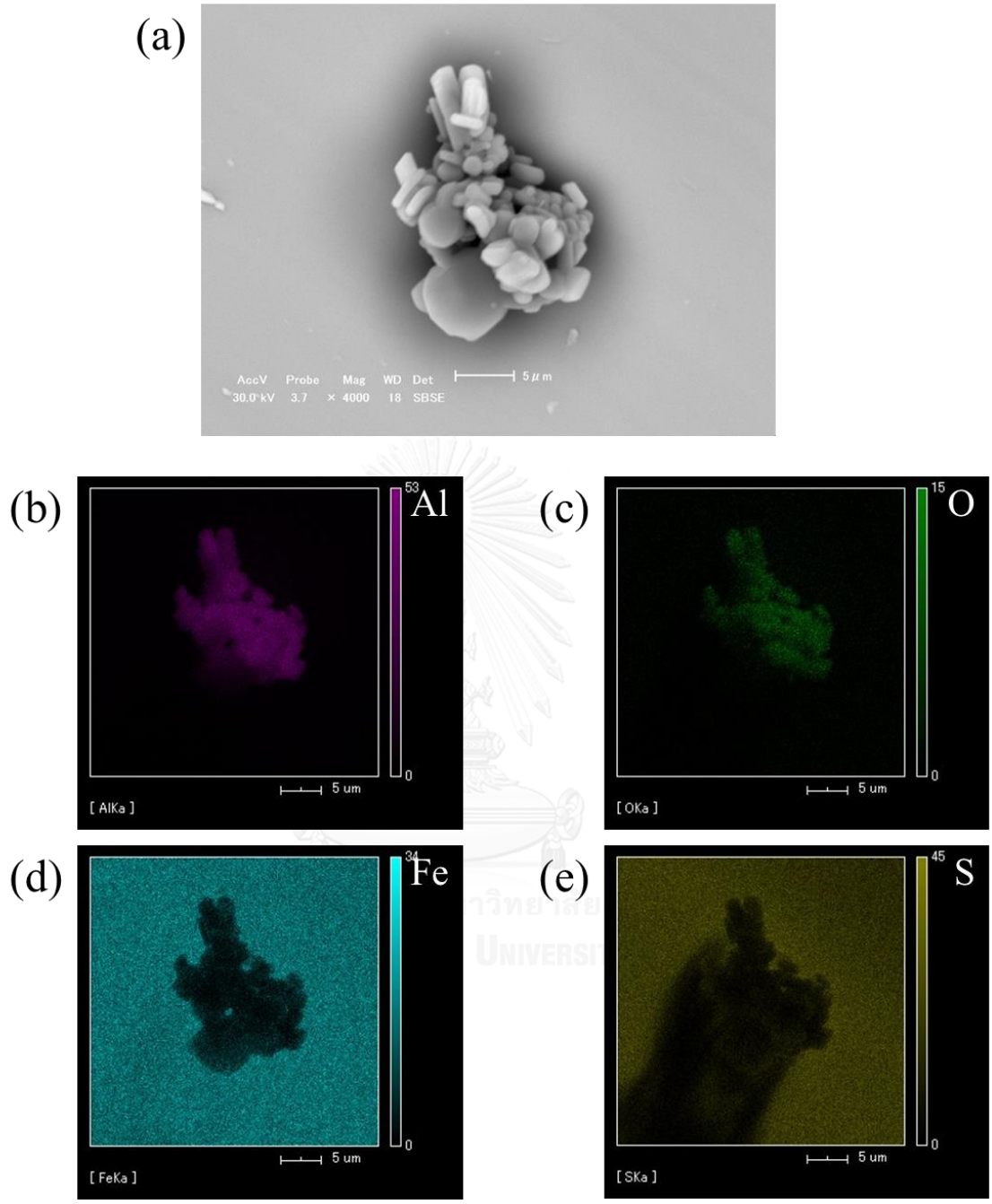

Figure 4-22 SEM photomicrograph of alumina particle attached onto pyrite surface after 7 days at with elemental maps of Al(b), O (c), Fe (d), and S (e) of the particle

Batch-type experiment was conducted by shaking pyrite in deionized water as control and in 200 mg/l alumina suspension to evaluate the effects of alumina on the net oxidation of pyrite (Figure 4-23). In the presence of alumina, the pH also decreased with time similar to that in deionized water. However, the pH values were statistically higher in the alumina suspension compared with deionized water (Figure 4-23a), which could be explained by the consumption of H^+ because of the dissolution of alumina (Figure 4-23e).

Alumina is insoluble in water, but it is slowly dissolved under acidic environments. Dissolution of alumina in acidic condition, which occurs after hydration of alumina and adsorption of H^+ (Franke, Ernst, & Myerson, 1987). The overall reaction of alumina dissolution process can be summarized in Equation (3-1), which illustrated that the dissolution of one Al^{3+} ion consumes three H^+ ions.

$$Al_2O_3 + 6\ H^+ \rightarrow 2\ Al^{3+} + 3\ H_2O \qquad \text{Equation (3-1)}$$

In the presence of alumina, dissolved S leached from pyrite increased, implying that pyrite oxidation was enhanced (Figure 4-23c). In contrast, dissolved Fe concentrations in the two cases were statistically the same (Figure 4-23d). The enhanced oxidation of pyrite in the alumina suspension could be attributed to faster oxidation of Fe^{2+} to Fe^{3+} at higher pH values (Evangelou, 1995). The generated Fe^{3+} could play a crucial role in the overall pyrite dissolution dynamics because the cathodic half-cell reaction is considered to be the "rate determining step" of pyrite oxidation (Rimstidt & Vaughan, 2003). However, the increase in pyrite dissolution was not visible in the dissolved Fe plots because Fe is very reactive under the pH conditions of the experiments and could easily precipitate to $Fe(OH)_3$. The evidence for this can be observed clearly with the plots of dissolved S compared with dissolved Fe in terms of molar concentration scale (Figure 4-24).

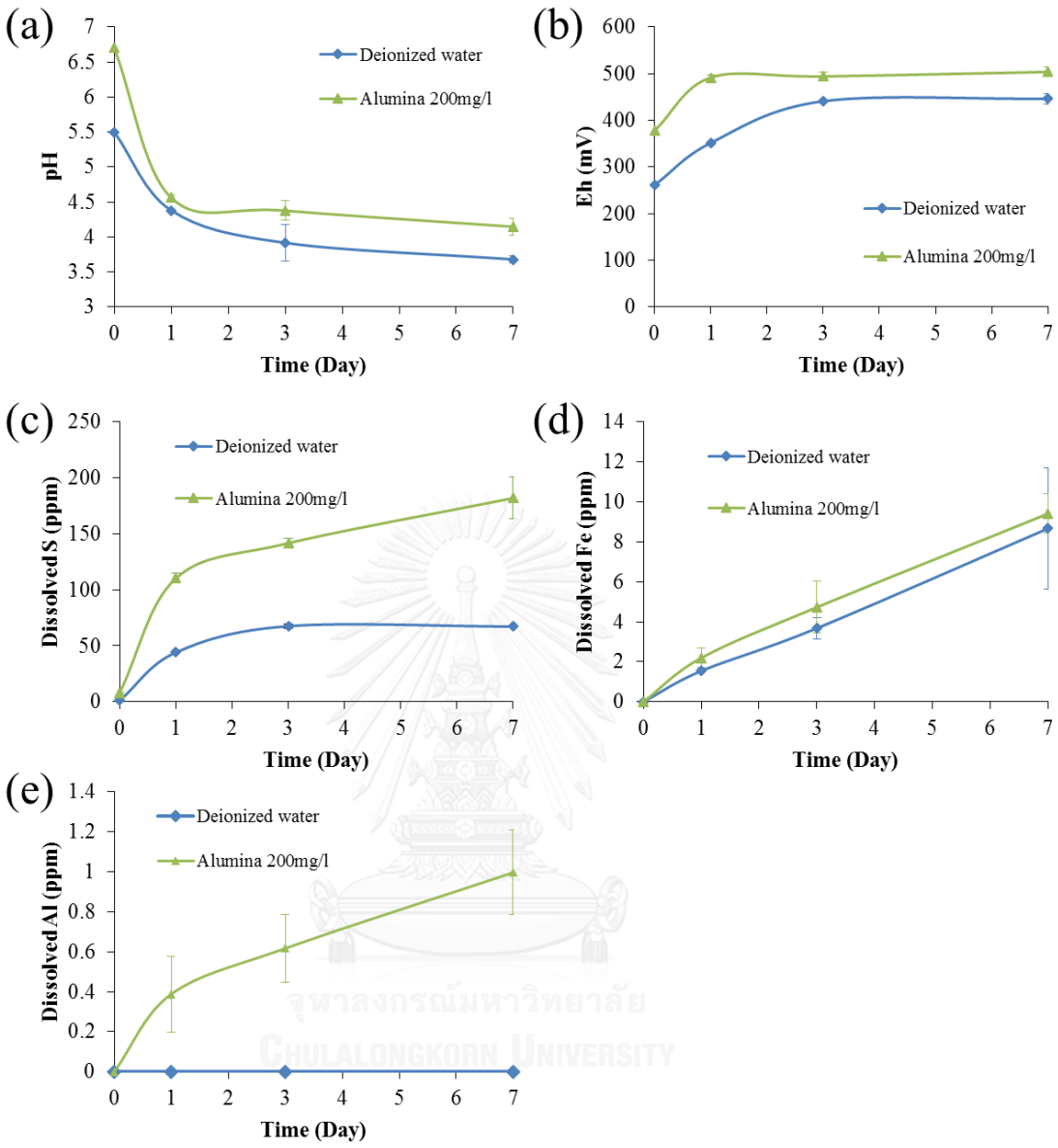

Figure 4-23 Changes of pH, Eh, and concentrations of dissolved S, Fe and Al with time in deionized water and alumina suspension: (a) pH change with time, (b) Eh change with time, (c) dissolved S concentration in ppm change with time, (d) dissolved Fe concentration in ppm change with time, and (e) dissolved Al concentration in ppm change with time

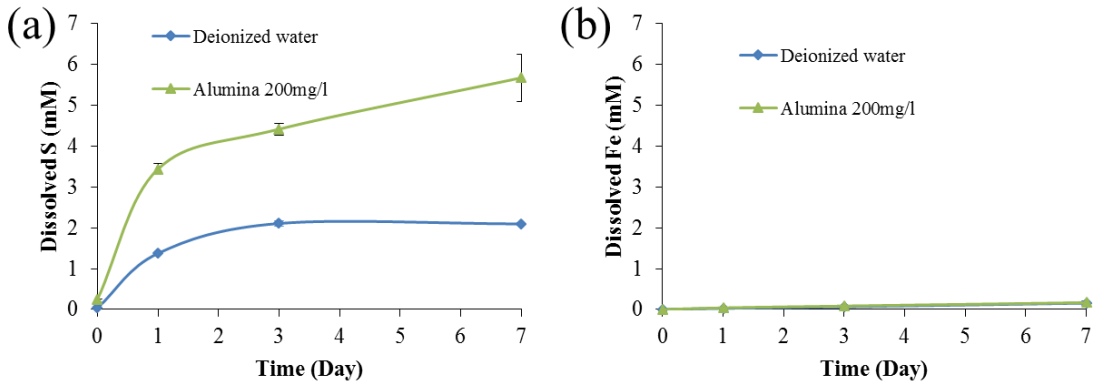

Figure 4-24 Changes of concentrations of dissolved S and Fe with time in deionized water and alumina suspension: (a) dissolved S concentration in mM change with time, and (b) dissolved Fe concentration in mM change with time

Figure 4-25 illustrates pH-Eh diagram based on actual concentration of dissolved Al, Fe and S measured in the batch experiments of pyrite in alumina suspension after 7 days. Based on thermodynamic considerations, the dissolved Al in the solution exist as $Al(OH)_3$ as it reaches equilibrium.

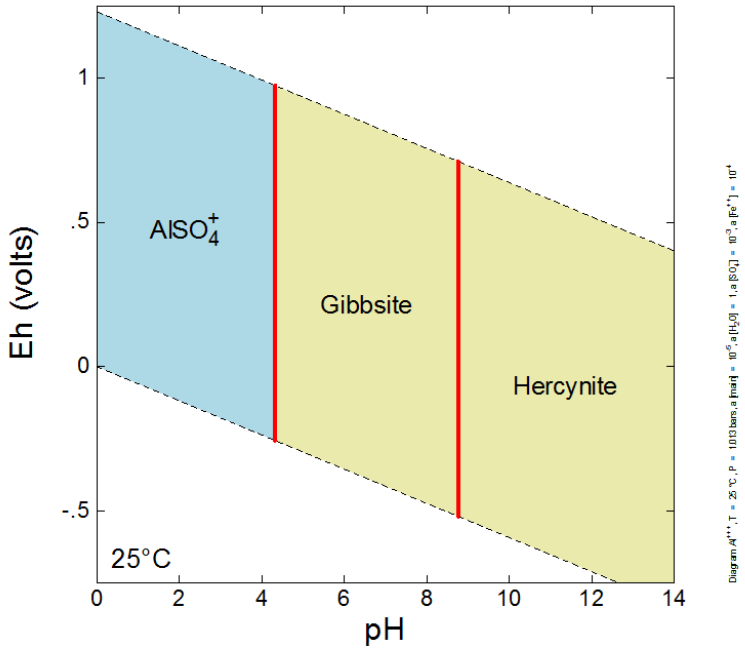

Figure 4-25 pH-Eh diagram of batch-type experiment with alumina (25 °C; activity of Al = 10^{-5}; activity of Fe = 10^{-4}; activity of S = 10^{-3})

DRIFTS spectra of pyrite after the batch experiments are shown in figure 4-26. Dashed line indicates spectra of pyrite surface species after leaching in deionized water for 7 days. There were also evidences of common oxidation products of pyrite, which are assigned to sulfate and its association with Fe^{3+} in the absorption range of 900-1200 cm^{-1} and sulfoxy anions (*e.g.*, SO_3^{2-}, $S_2O_3^{2-}$, $S_nO_6^{2-}$) around absorption band of 600-800 cm^{-1} as explained above. In the case of oxidation products in the presence of alumina, aside from the absorption bands similar to the previous case, peaks in the region of 3500-3700 cm^{-1} could refer to surface hydroxyl groups on as-received alumina powders (Lee & Condrate, 1995). These peaks were less prominent because alumina particles did not cover the surface of pyrite. There were also additional absorption peaks at 678 and 655 cm^{-1} that could be attributed to the presence of Al-OH^- (Ram, 2001). The result suggests that dissolved Al can associate with other functional groups and adsorbed onto the pyrite surface. In the next section, we investigated their electrochemical effects on pyrite dissolution process in greater detail.

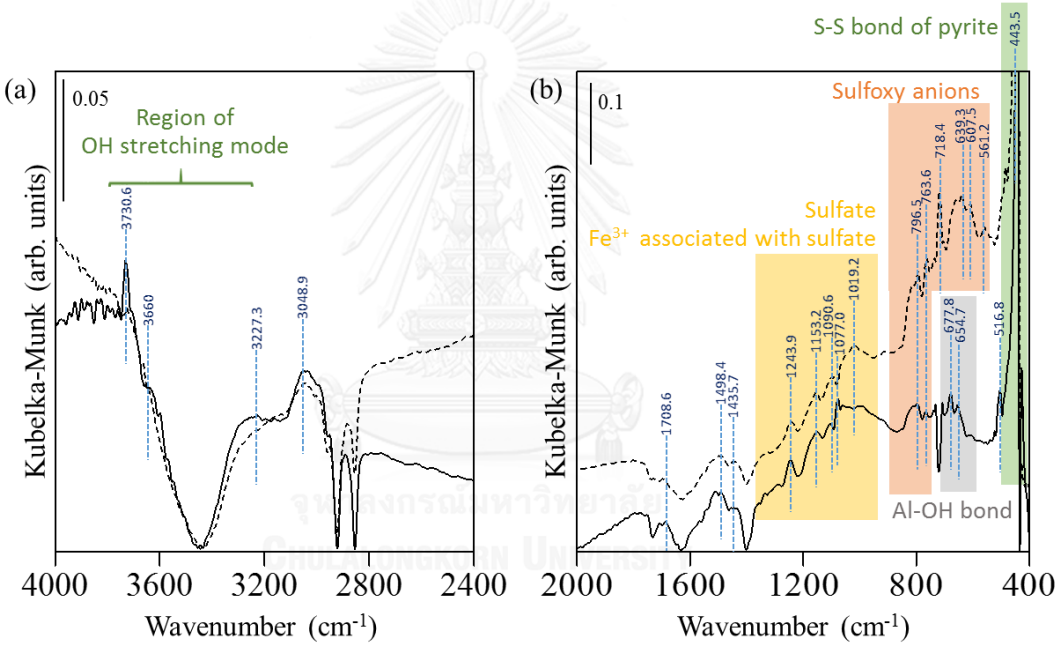

Figure 4-26 DRIFTS spectra of washed pyrite and pyrite after leaching for 7 days at 25 °C in alumina suspension (solid line) and deionized water (dashed line)

4.3.2 Electrochemical study of the effects of alumina on pyrite dissolution

Figure 4-27 illustrates cyclic voltammograms of polished pyrite and those oxidized in air, deionized water and 200 mg/l alumina suspension for 24 hours. In comparison to the CV of pyrite in other cases, CV of pyrite treated in alumina suspension shows different current density profile. Higher current density was observed during the anodic sweep but the reduction peak of Fe^{3+} to Fe^{2+} at + 0.4 V remained undisturbed compared to the previous case of deionized water. Moreover, additional cathodic current between -0.2 and +0.2 V can be observed in the case of alumina suspension treated pyrite. Therefore, there could be additional reactions occurring exclusively to the case of alumina. One possible explanation for this is that during the anodic sweep, the O^{2-} component in alumina underwent oxidation, resulting in the

formation of dissolved O_2 near the pyrite surface and the generated O_2 also further enhanced the oxidative decomposition of sulfoxy anions as observed in higher current density profile. This deduction is supported by the appearance of an additional cathodic peak between -0.2 and +0.2 V that is consistent with the reduction of dissolved O_2 as this pattern of cathodic current density was also observed in CV under oxic condition (Figure 4-4).

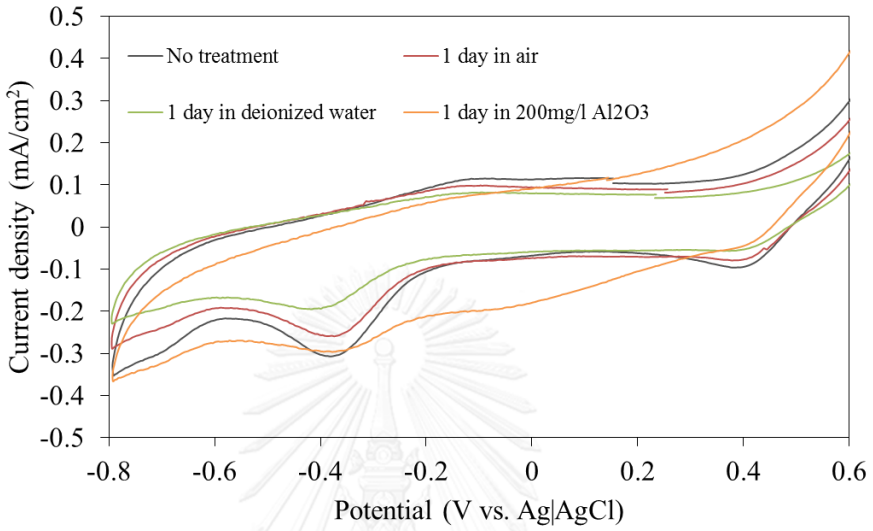

Figure 4-27 Cyclic voltammogram of polished pyrite and pyrite exposed to air, DI water and alumina suspensions for 24 hours (2nd cycle; Sweep rate 30 mV/s; 25 °C; anoxic condition; no agitation)

Figure 4-28 illustrates anodic polarization current density profile at fixed potential of +0.6 V vs Ag|AgCl of pyrite oxidized in deionized water and 200 mg/l alumina suspension. The result indicates that higher oxidation during the anodic polarization in the case of pyrite treated in 200 mg/l alumina suspension for 24 hours could be the result of enhancement of the anodic half-cell reaction of pyrite dissolution by the presence of alumina. Similar to the case of hematite, this enhancement effect might influence the interaction between pyrite and Fe-oxyhydroxides as the equilibrium of both case are identical in intensity. The extra source of Fe-oxyhydroxides on pyrite surface, which leads to more oxidative reactions, was most likely because pyrite dissolution was more extensive in the presence of alumina as explained by the batch experimental results (Figure 4-23).

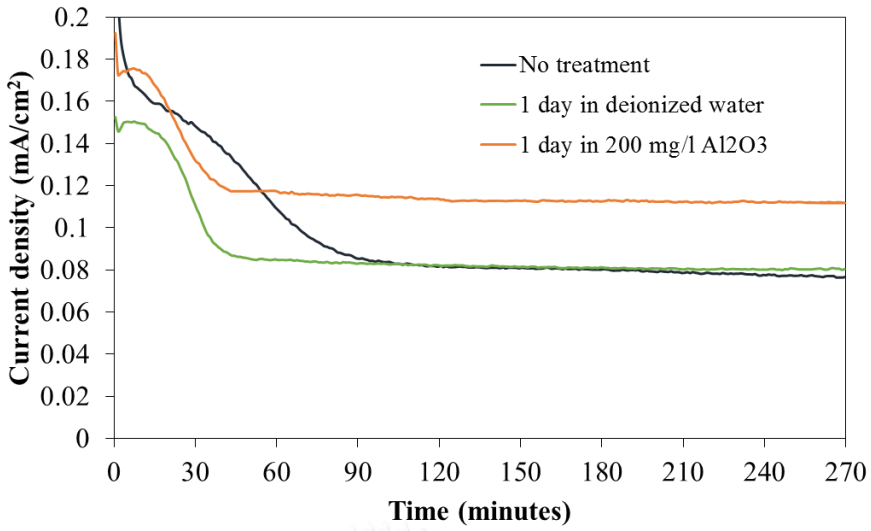

Figure 4-28 Anodic polarization of polished pyrite and pyrite exposed to DI water and alumina suspension for 24 hours (Potential +0.6 V vs Ag|AgCl; 25 °C; anoxic condition; 250 rpm agitation)

Figure 4-29 illustrates cathodic polarization profile of pyrite oxidized in 20 mg/l alumina suspension and 200 mg/l hematite suspension for 24 hours at the potential of -0.2 V vs Ag|AgCl. The result shows sign of decreases in intensity of current density with higher amount of alumina on pyrite surface. Similar to the case with hematite, the reason for this might be because alumina attached on pyrite surface physically "protect" pyrite from oxidants (i.e. O_2 and Fe^{3+}), which is the main source of cathodic current during the measurement.

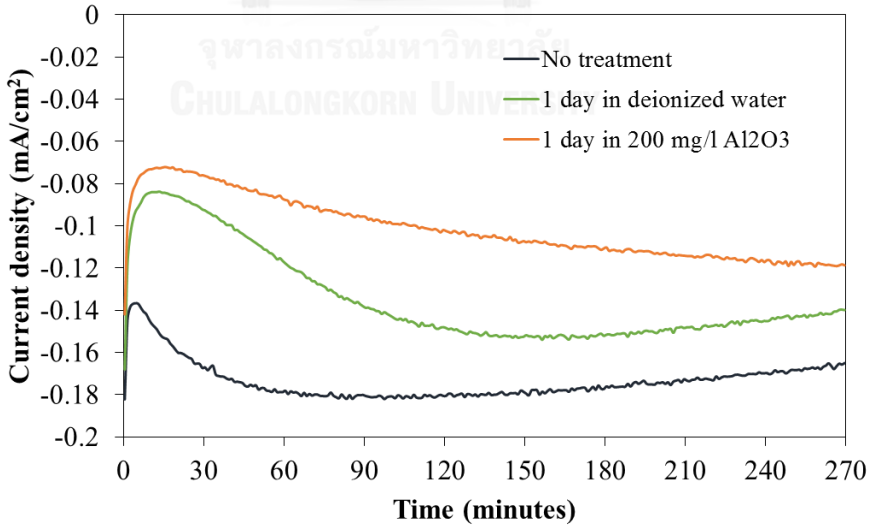

Figure 4-29 Cathodic polarization of polished pyrite and pyrite exposed to DI water and alumina suspension for 24 hours (Potential -0.2 V vs Ag|AgCl; 25 °C; oxic condition; 250 rpm agitation)

CHAPTER 5
CONCLUSIONS

Pyrite mineral (FeS_2), the most abundant metal sulfide mineral found in various geological formations around the world, is responsible for the formation of acid mine drainage (AMD) which is one of the most serious anthropogenic environmental impacts from mining and mineral processing activities. In the mining perspective, the abundance pyrite is usually rejected as gangue mineral due to its low economic value and goes to overburden pile or tailings dam along with waste rocks and other gangue minerals. Upon exposure to atmospheric conditions, pyrite would be electrochemically dissolved and releases highly acidic leachate contaminated with various hazardous elements (i.e. heavy metal contaminations), which affects ecosystem and also well-being of stakeholders nearby. The purpose of present study was to investigate greater details in electrochemical behavior of pyrite and its interaction with metal oxides or metal-organic complexes.

Briefly introduction of AMD and its environmental concerns was mentioned in chapter 1, and study reviews of mechanism of pyrite dissolution including some AMD remediation options were summarized in chapter 2.

Chapter 3 described the materials and methodology used for the study of effects of metal oxides on pyrite dissolution. In this study, the attachment of metal oxide particles on the pyrite surface was investigated with zeta potential measurement and confirmed with microscopic images from light microscope and SEM-EDX. Effects of the metal oxides on pyrite dissolution dynamics were investigated in batch-type leaching experiment, and then identified oxidation products on the pyrite surface with Fourier Transform Infrared Spectroscopy (DRIFTS). The results are also supported with geochemical modelling calculations based on the actual concentrations measured.

Chapter 4 reported the study on effects of common metal oxides, like hematite (α-Fe_2O_3) and alumina (α-Al_2O_3), which naturally come to contact with pyrite at the AMD contaminated sites. The hematite (α-Fe_2O_3) was selected for studying effects of metal oxide on pyrite dissolution because it was reported as one of the main thermodynamically stable final products formed on the pyrite surface (Schwertmann, Friedl, & Stanjek, 1999). Meanwhile the alumina (α-Al_2O_3) was selected for the study due to environmental perspective. As alumino-silicate minerals (*i.e.* feldspars and kaolinite) are very common in nature, alumina was expected to play important role in pyrite dissolution dynamics as well.

The effects on each of the half-cell reaction of pyrite dissolution process are further elucidated with electrochemical experiments (cyclic voltammetry and chronoamperometry) done with pyrite single crystal working electrode. The results of batch experiment indicate that acidity (pH) of the leachate decreased with time and

reached apparent equilibrium after 3 days of shaking at the chosen condition. It was found that dissolved S in the leachate could be used as an indicator to evaluate the degree of dissolution of pyrite as dissolved Fe concentration were likely to be controlled by pH.

The study on effects of hematite on pyrite dissolution dynamics found that, with the presence of hematite particles on pyrite, the pyrite dissolution was suppressed without any influence on evolution of pH. Despite, the anodic half-cell reaction of pyrite could be enhanced by the presence of hematite by the "bridging effect" of the particles, while the cathodic half-cell reaction could be suppressed as the pyrite's exposure to oxidants (*i.e.* O_2 and Fe^{3+}) was reduced by physical protection of the attached particles. These results can be considered that suppression in cathodic half-cell reaction with the presence of hematite would result in reduction of the net reaction observed in batch experiment, as the cathodic half-cell reaction of pyrite dissolution process was reported to be "rate determining step" (Rimstidt & Vaughan, 2003).

For the effects of alumina on pyrite dissolution dynamics, pH of the leachate was slightly higher with the presence of alumina compared to the control case, as resulted from buffering effect from dissolution of alumina in acidic environment. This relative higher pH value led to enhancement in pyrite dissolution rate. In this case, the anodic half-cell reaction of pyrite was also enhanced as more Ferric Oxy-hydroxide with similar "bridging effect" were formed on pyrite surface during the treatment with alumina suspension. Similar to the case of hematite, the cathodic half-cell reaction was found to be suppressed as well. Even the effects of hematite and alumina on each of the half-cell reactions were in the same trend, the effect on net reaction was different. This contradiction might occurred because the interpretation of electrochemical study is pH-sensitive.

In addition, a fundamental electrochemical study of the redox behavior of metal-organic complexes like Ti- and Si-catechol complexes, which are critical variables during carrier microencapsulation (CME), was preliminary conducted and shown in appendix. The results showed that either free-catechol or metal-catechol complexes are more redox reactive on the surface of pyrite. The formation of redox-reactive Ti- and Si-catechol complexes under alkaline conditions was also confirmed.

Although Si-catechol complexes were not formed at pH 3, the results suggest that a relatively stable Ti-catechol complex might have been formed under this pH condition. However, more experiments are still needed to identify this complex and understand the reasons why it reacted strongly on the pyrite surface.

REFERENCES

Abraitis, P., Pattrick, R., & Vaughan, D. (2004). Variations in the compositional, textural and electrical properties of natural pyrite: a review. *International Journal of Mineral Processing, 74*(1), 41-59.

Akcil, A., & Koldas, S. (2006). Acid mine drainage (AMD): causes, treatment and case studies. *Journal of Cleaner Production, 14*(12), 1139-1145.

Borgias, B. A., Cooper, S. R., Koh, Y. B., & Raymond, K. N. (1984). Synthetic, structural, and physical studies of titanium complexes of catechol and 3, 5-di-tert-butylcatechol. *Inorganic Chemistry, 23*(8), 1009-1016.

Chandra, A., & Gerson, A. R. (2010). The mechanisms of pyrite oxidation and leaching: a fundamental perspective. *Surface Science Reports, 65*(9), 293-315.

Egiebor, N. O., & Oni, B. (2007). Acid rock drainage formation and treatment: a review. *Asia-Pacific Journal of Chemical Engineering, 2*(1), 47-62.

Evangelou, V. (1995). *Pyrite oxidation and its control*: CRC press.

Evangelou, V. (2001). Pyrite microencapsulation technologies: principles and potential field application. *Ecological Engineering, 17*(2), 165-178.

Fornasiero, D., Eijt, V., & Ralston, J. (1992). An electrokinetic study of pyrite oxidation. *Colloids and Surfaces, 62*(1-2), 63-73.

Franke, M. D., Ernst, W., & Myerson, A. (1987). Kinetics of dissolution of alumina in acidic solution. *AIChE journal, 33*(2), 267-273.

Gray, N. (1997). Environmental impact and remediation of acid mine drainage: a management problem. *Environmental Geology, 30*(1-2), 62-71.

Hu, G., Dam-Johansen, K., Wedel, S., & Hansen, J. P. (2006). Decomposition and oxidation of pyrite. *Progress in Energy and Combustion Science, 32*(3), 295-314.

Järup, L. (2003). Hazards of heavy metal contamination. *British medical bulletin, 68*(1), 167-182.

Jha, R. K. T., Satur, J., Hiroyoshi, N., Ito, M., & Tsunekawa, M. (2008). Carrier-microencapsulation using Si–catechol complex for suppressing pyrite floatability. *Minerals Engineering, 21*(12), 889-893.

Jha, R. K. T., Satur, J., Hiroyoshi, N., Ito, M., & Tsunekawa, M. (2011). Suppression of floatability of pyrite in coal processing by carrier microencapsulation. *Fuel processing technology, 92*(5), 1032-1036.

Johnson, D. B., & Hallberg, K. B. (2005). Acid mine drainage remediation options: a review. *Science of the total environment, 338*(1), 3-14.

Kelsall, G., Yin, Q., Vaughan, D., England, K., & Brandon, N. (1999). Electrochemical oxidation of pyrite (FeS 2) in aqueous electrolytes. *Journal of Electroanalytical Chemistry, 471*(2), 116-125.

Lee, D., & Condrate, R. (1995). An FTIR spectral investigation of the structural species found on alumina surfaces. *Materials Letters, 23*(4), 241-246.

Lowson, R. T. (1982). Aqueous oxidation of pyrite by molecular oxygen. *Chemical Reviews, 82*(5), 461-497.

McKibben, M. A., & Barnes, H. L. (1986). Oxidation of pyrite in low temperature acidic solutions: Rate laws and surface textures. *Geochimica et Cosmochimica Acta, 50*(7), 1509-1520.

Mishra, K., & Osseo-Asare, K. (1988). Aspects of the interfacial electrochemistry of semiconductor pyrite (FeS2). *Journal of The Electrochemical Society, 135*(10), 2502-2509.

Murphy, R., & Strongin, D. R. (2009). Surface reactivity of pyrite and related sulfides. *Surface Science Reports, 64*(1), 1-45.

Nair, N. N., Schreiner, E., & Marx, D. (2006). Glycine at the pyrite-water interface: The role of surface defects. *Journal of the American Chemical Society, 128*(42), 13815-13826.

Ohman, L.-O., Nordin, A., Sedeh, I. F., & Sjoberg, S. (1991). Equilibrium and Structural Studies of Silicon (IV) and Aluminium (lll) in Aqueous Solution. 28. Formation of Soluble Silicic Acid-Ligand Complexes as Studied by Potentiometrie and Solubility Measurements. *Acta chemica scandinavica, 45*, 335-341.

Ram, S. (2001). Infrared spectral study of molecular vibrations in amorphous, nanocrystalline and AlO (OH)· αH 2 O bulk crystals. *Infrared physics & technology, 42*(6), 547-560.

Reedy, B. J., Beattie, J. K., & Lowson, R. T. (1991). A vibrational spectroscopic 18O tracer study of pyrite oxidation. *Geochimica et Cosmochimica Acta, 55*(6), 1609-1614.

Rimstidt, J. D., & Vaughan, D. J. (2003). Pyrite oxidation: a state-of-the-art assessment of the reaction mechanism. *Geochimica et Cosmochimica Acta, 67*(5), 873-880.

Rosso, K. M., Becker, U., & Hochella, M. F. (1999). The interaction of pyrite {100} surfaces with O2 and H2O: Fundamental oxidation mechanisms. *American Mineralogist, 84*(10), 1549-1561.

Satur, J., Hiroyoshi, N., Tsunekawa, M., Ito, M., & Okamoto, H. (2007). Carrier-microencapsulation for preventing pyrite oxidation. *International Journal of Mineral Processing, 83*(3), 116-124.

Schweigert, N., Zehnder, A. J., & Eggen, R. I. (2001). Chemical properties of catechols and their molecular modes of toxic action in cells, from microorganisms to mammals. *Environmental Microbiology, 3*(2), 81-91.

Schwertmann, U., Friedl, J., & Stanjek, H. (1999). From Fe (III) ions to ferrihydrite and then to hematite. *Journal of Colloid and Interface Science, 209*(1), 215-223.

Singer, P. C., & Stumm, W. (1970). Acidic mine drainage: the rate-determining step. *Science, 167*(3921), 1121-1123.

Tabelin, C. B., Igarashi, T., Tamoto, S., & Takahashi, R. (2012). The roles of pyrite and calcite in the mobilization of arsenic and lead from hydrothermally altered rocks excavated in Hokkaido, Japan. *Journal of Geochemical Exploration, 119*, 17-31.

Taylor, S. (1964). Abundance of chemical elements in the continental crust: a new table. *Geochimica et Cosmochimica Acta, 28*(8), 1273-1285.

Thakur Jha, R. K., Satur, J., Hiroyoshi, N., Ito, M., & Tsunekawa, M. (2012). Suppression of pyrite oxidation by carrier microencapsulation using silicon and catechol. *Mineral Processing and Extractive Metallurgy Review, 33*(2), 89-98.

Williamson, M. A., & Rimstidt, J. D. (1994). The kinetics and electrochemical rate-determining step of aqueous pyrite oxidation. *Geochimica et Cosmochimica Acta, 58*(24), 5443-5454.

APPENDIX

CARRIER MICROENCAPSULATION – ELECTROCHEMICAL STABILITIES OF METAL-ORGANIC COMPLEXES

As discussed in **Chapter 2**, Carrier Microencapsulation (CME) utilizes metal-organic complexes to suppress pyrite oxidation through their redox properties.

Methodology

Cyclic voltammetry experiments were conducted in the same manner as in **Chapter 3**. Characterization of pyrite sample and pyrite working electrode making procedure are identical and were also described in **Chapter 3**.

In the investigation of stability of free-catechol and metal-catechol complexes, a platinum electrode (surface area: 7.06 mm^2) was used. In contrast, a pyrite electrode was used to investigate the effects of free-catechol and metal-catechol complexes on pyrite oxidation. All measurements started from the open circuit potential (OCP) toward anodic direction (*i.e.*, positive potential). Sweep rates for the scans were set at 5 mV/s and 30 mV/s for measurements done on platinum and pyrite electrodes, respectively.

Table A1. Compositions of solutions for cyclic voltammetry

Cases	***Compositions of the solutions***	***pH***
Ti-catechol complex	*2mM Ti, 6mM catechol, 0.1M Na_2SO_4*	*3.0 and 9.0*
Si-catechol complex	*2mM Si, 6mM catechol, 0.1M Na_2SO_4*	*3.0 and 9.0*
Background: Ti^{4+}	*2mM Ti, 0.1M Na_2SO_4*	*3.0 and 9.0*
Background: Si^{4+}	*2mM Si, 0.1M Na_2SO_4*	*3.0 and 9.0*
Free-catechol	*6mM catechol, 0.1M Na_2SO_4*	*3.0 and 9.0*
Background: CO_3^{2-}	*2mM Na_2CO_3, 0.1M Na_2SO_4*	*3.0 and 9.0*
Pyrite oxidation background	*0.1M Na_2SO_4 (natural pH)*	*5.8*

Metal-catechol complexes were prepared by mixing reagent-grade solutions of Ti and Si ions ($Ti(SO_4)_2$ in H_2SO_4 or Na_2SiO_3 in Na_2CO_3, Wako Chemical Co. Ltd., Japan), catechol (Wako Chemical Co. Ltd., Japan) and Na_2SO_4 as supporting electrolyte (Table A1). The pH of these solutions were adjusted using H_2SO_4 or NaOH solutions and filtered through 0.2 µm syringe-type membrane filters (Sartorius AG, Germany) to remove metal-oxyhydroxide precipitates or "polymerized" organic molecules. Prior to each measurement, the solution was poured into the electrochemical cell with constant temperature water jacket (25°C) and allowed to equilibrate for at least 40 minutes. After this, the solution was purged with nitrogen gas for at least 20 minutes to remove dissolved O_2. Nitrogen gas was also continuously introduced over the electrolyte

throughout the measurements to maintain anoxic conditions. Measurements of background species (*i.e.*, Ti^{4+}, Si^{4+} and CO_3^{2-}) were also done for reference.

Stability of free-catechol and metal-catechol complexes on platinum

Cyclic voltammograms of catechol on a platinum electrode showed approximately equal current densities measured over 5 cycles (data not shown) with a peak at ca. 0.5 V during the anodic sweep and another one at 0.35 V during the cathodic sweep. The anodic and cathodic peaks could be attributed to the oxidation of catechol to quinone (1,2-Benzoquinone) and the reduction of quinone to catechol, respectively (Schweigert, Zehnder, & Eggen, 2001). The anodic and cathodic peaks at pH 3 were slightly higher than those at pH 9 (Figure A1). This means that free-catechol is more reactive under acidic than alkaline conditions. It is interesting to note that under both pH conditions, the cathodic peak was much smaller than the anodic peak, which suggest that only some of the quinone could be reduced back to catechol.

Catechol and Ti^{4+}could form a Ti-catechol complex, $Ti(cat)_3^{2-}$, that is stable between pH 6-12 (Borgias, Cooper, Koh, & Raymond, 1984). In our experiments, substantially lower cathodic and anodic peaks were observed at pH 3 (Figures A1-a1 and A1-a2). There are two possibilities for this discrepancy: (1) free-catechol in the solution decreased due to its enhanced oxidation in the presence of metal ions like Ti^{4+} (Schweigert et al., 2001), and (2) some Ti-cat complex was formed that is relatively stable under acidic conditions. The second possibility will be discussed in more detail in the next subsection. Under alkaline conditions, two peaks appeared on the anodic sweep that were higher than that under acidic condition (Figures A1-a1 and A1-b1). In addition, these "compound" peak decreased after each cycle and shifted towards more positive potentials. These indicate that some kind of new compound was formed that is more reactive under alkaline condition. This new compound is most likely $Ti(cat)_3^{2-}$ as reported by (Borgias et al., 1984). This same complex was also indirectly observed in the work of Satur *et al.* (2009) on rutile and anatase. These results indicate that $Ti(cat)_3^{2-}$ could be formed at pH 9, and it is more easily oxidized under alkaline conditions.

The cyclic voltammetry results of Si-catechol solution at pH 3 (Figure A2-a) shows that the anodic and cathodic peaks of the Si-cat mixture and free-catechol were almost the same. This means that Si-catechol complexes were not formed at pH 3 and in contrast to Ti^{4+}, the effects of Si^{4+} ions on the oxidation of catechol was negligible. At pH 9, a wide, probably "compound" peak was observed, but was lower than that of free-catechol (Figure A2-b). This suggest that a Si-catechol complex was formed but was most likely less reactive than free-catechol. A tris-catecholato complex of Si^{4+} ($Si(cat)_3^{2-}$) is formed at pH greater than 7.5 in a Si-catechol system, which is consistent with our result. (Ohman, Nordin, Sedeh, & Sjoberg, 1991).

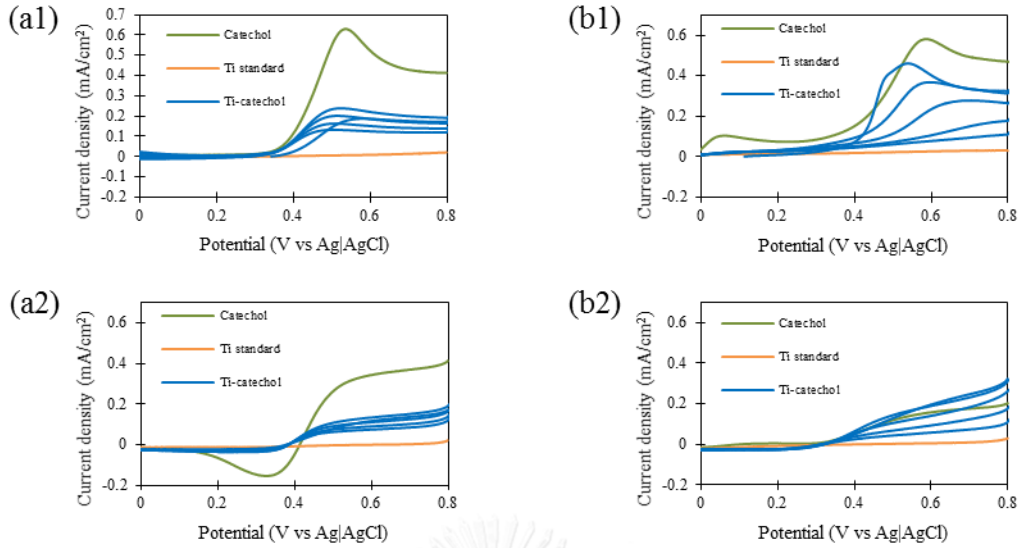

Figure A1 Cyclic voltammograms of Ti-catechol complex and background measurements on platinum electrode of; (a1) anodic sweep in acidic condition (pH 3.0), (b1) anodic sweep in alkaline condition (pH9.0), (a2) cathodic sweep in acidic condition (pH 3.0), (b2) cathodic sweep in alkaline condition (pH 9.0)

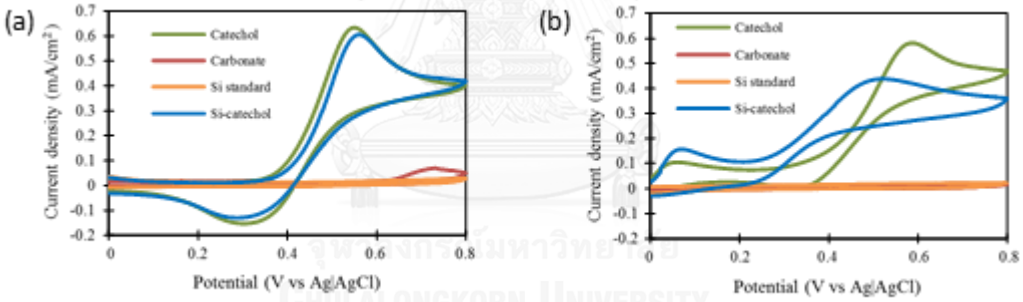

Figure A2 Cyclic voltammograms of Si-catechol complex and background measurements on platinum electrode [2nd cycle] in; (a) acidic condition (pH 3.0), and (b) alkaline condition (pH9.0)

Stability of free-catechol and metal-catechol complexes on pyrite

Cyclic voltammetry results of free-catechol on the pyrite electrode (Figures A3 and 6) shows higher amplitude of observed current density compared to the platinum electrode (Figures A1 and A2). In addition, higher peaks were measured at pH 3 than pH 9. This means that the pyrite surface was more reactive compared with platinum and the reactivity of catechol on pyrite was strongly pH dependent.

For the electrochemical reactions between pyrite and Ti-catechol complex (Figure A3), the anodic peaks in both pH conditions decreased and shifted towards the left. As mentioned above, there is a possibility that a Ti-catechol complex was formed, but this complex is not so reactive under acidic conditions. The identical shifting of the peaks towards lower potentials in both pH 3 and 9 indicates that such a Ti-catechol complex might be present in the system. The surface of pyrite is more reactive than that

platinum so there is a strong possibility that pyrite may have mediated in the oxidation of this complex under acidic conditions (Figures A1 and A2). On the other hand, the lower current densities during the anodic sweeps could be attributed and the corresponding less negative current density during the cathodic sweep in pH 9 could be attributed to the gradual passivation of the pyrite surface (Satur et al., 2007). Take note that at pH 3, the current density decrease in the anodic sweep was followed by a corresponding more negative current density during the cathodic sweep. A more negative cathodic sweep means that the reduction of oxidants was higher. This means that passivation of pyrite by Ti-catechol complexes was more efficient under alkaline conditions.

The cyclic voltammetry of Si-catechol complex on pyrite at pH 3 is illustrated in Figure A4-a. This trend is identical to that observed on platinum (Figure A2-a) indicating that the current density increase during the anodic sweep was due to free-catechol. At pH 9, the anodic sweep shifted to lower potentials similar to Ti-catechol complex and another peak appeared between 0 and 0.2 V. This means that Si-catechol complexes reacts stronger on the surface of pyrite than Ti-catechol complex. Moreover, Si-catechol complex at pH 9 reduced the current density during the anodic sweep with a corresponding less negative current density on the cathodic sweep, indicating that it also passivated pyrite similar to Ti-catechol complex. These results suggest that free-catechol and metal-catechol complexes strongly influenced the overall dynamics of pyrite oxidation by interacting with both the cathodic and anodic sites formed on the pyrite surface

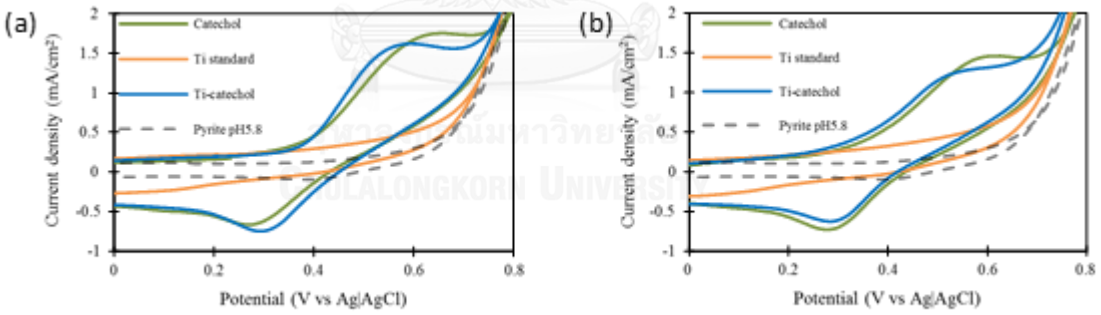

Figure A3 Cyclic voltammograms of Ti-catechol complex and background measurements on pyrite electrode [2nd cycle] in; (a) acidic condition (pH 3.0), and (b) alkaline condition (pH9.0)

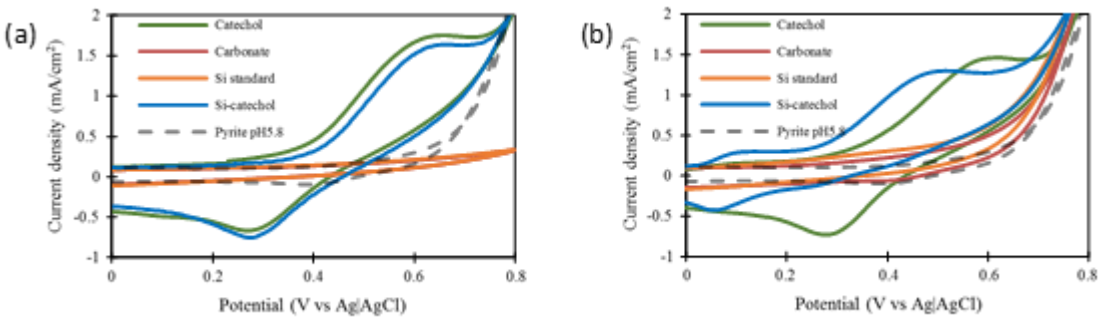

Figure A4 Cyclic voltammograms of Si-catechol complex and background measurements on pyrite electrode [2nd cycle] in; (a) acidic condition (pH 3.0), and (b) alkaline condition (pH9.0)

VITA

Suchol Veerawattananun was born in Bangkok, Thailand on July 30, 1992. He graduated in 2014 with Bachelor of Engineering (2nd class honours) in Georesources Engineering from Department of Mining and Petroleum Engineering, Faculty of Engineering, Chulalongkorn University, Thailand. Then, he continued his educational career with Masters of Engineering in Georesources Engineering at the same department. Between June 2015 and February 2016, he was exchanged at Laboratory of Mineral Processing and Resources Recycling, Division of Sustainable Resources Engineering, Graduate School of Engineering, Hokkaido University with supports from the graduate program for fostering frontiers of practical solutions in a Population-Activities-Resources-Environments (PARE) chain. He was awarded with the Masters of Engineering degree in 2016.